Studies on Bioactivity and Molecular Mechanism of *Bifidobacterium longum* on Anti-aging in *Caenorhabditis elegans*

January 2021

Takaya SUGAWARA

Studies on Bioactivity and Molecular Mechanism of *Bifidobacterium longum* on Anti-aging in *Caenorhabditis elegans*

A Dissertation Submitted to
the Graduate School of Life and Environmental Sciences,
the University of Tsukuba
in Partial Fulfillment of the Requirements
for the Degree of Doctor of Philosophy in Science
(Doctoral Program in Biological Sciences)

Takaya SUGAWARA

Table of contents

Abbreviation

ATP: adenosine triphosphate
BL: Bifidobacterium longum
CGC: caenorhabditis genetics center
CRISPR: Clustered Regularly Interspaced Short Palindromic Repeats
DAF: dauer abnormal formation
DCCD: N,N-dicyclohexylcarbodiimide
DCF-DA: 2',7'-dichlorodihydrofluorescein diacetate
DMSO: dimethyl sulfoxide
FUdR: fluorodeoxyuridine
dDW: double distilled water
GFP: green fluorescent protein
GPX: Glutathione peroxidase
GST: glutathione S-transferase
HSF: heat shock factor
HSP: heat shock protein
IGF: insulin-like growth factor
IIS: insulin/IGF-1 signaling
INS: insulin
JNK: c-Jun N-terminal kinase
LET: lethal
NBRP: national bioresource project
NGM: Nematode Growth Medium
Nrf: NF-E2-related factor
PHA: defective pharynx development
ROS: reactive oxygen species
MAPK: mitogen-activated protein kinase
PD: parkinson's disease
qPCR: quantitative polymerase chain reaction
SIRT: sirtuin
SKN: skinhead
SOD: superoxide dismutase
CTL: catalase
TLR: toll-like receptor
TOR: target of rapamycin
TTFA: 2-thenoyltrifluoroacetone
UV: ultraviolet

Abstract

In modern society, human life expectancy is increasing compared to the past, and the term "health span" is beginning to be used in addition to the term "life span". Although currently there is a gap between life span and health span, reducing the gap by extending health span is important to improve people's quality of life. In this study, I analyzed the effects of bifidobacterium on health and anti-aging as candidates for bioactive substances that can extend health span. In this study, *Caenorhabditis elegans* was used as an experimental model organism.

Bifidobacterium is a probiotics, which are beneficial microorganisms to humans, and is the highest percentage of probiotics in the human gut. As such, they have considerable influence on the host and have beneficial effects on human health, including improvement of intestinal flora. Currently, various physiological effects of bifidobacterium are known to enhance immune function, alleviate allergies, and inhibit cancer development. Although its physiological effects on anti-aging have also been reported, there are many unresolved aspects of its effects, which I sought to elucidate in this study.

C. elegans is widely used as a model organism for biological experiments because it is easy to breed. In addition, it has basic organs such as the intestines, nerves, and reproductive organs, which enable it to simulate the digestion and absorption of food extracts and functional substances.

Although several previous studies have analyzed the bioactive effects of bifidobacterium using nematodes, there are only a few studies on anti-aging and there are many unexplored aspects. In this study, I fed sterilized *Bifidobacterium longum* (BR-108, BL) together with *E. coli*, the food source of nematodes, in order to explore a new bioactive effect of *B. longum* on anti-aging and to elucidate the mechanism of its action.

C. elegans fed a mixture of BL and *E. coli* increased various stress tolerance compared to *C. elegans* fed only *E. coli*. BL increased the expression of genes related to stress tolerance, which in turn increased the stress tolerance, extended the lifespan and prevented the loss of motility with aging. I also measured muscle mass, ATP levels, mitochondrial mass and mitochondrial membrane potential, and ROS levels in nematodes for further analysis of the significant suppression of age-related motility loss and found that BL-induced change of these phenotypes were upregulated. It was suggested that the maintenance of motility was caused by the effects on muscle and mitochondria. Compared to BL-induced changes in muscle mass, mitochondrial mass and membrane potential were substantially increased. Therefore, I hypothesized that BL has a greater effect on mitochondria, which produce ATP for muscle energy, than on muscle, and I used mitochondrial complex inhibitors to search for mitochondrial target sites for BL-induced effects in mitochondria. Mitochondria have five complexes, I, II, III, IV and V and some of the inhibitors suppressed the increase in motility and mitochondrial membrane potential. Although the target sites have yet to be elucidated, it is suggested

that the mitochondrial electron transfer chain and ATP biosynthesis are important in the suppression of age-related decline of motility.

In order to analyze in more detail the mechanism of the bioactive activity of bifidobacterium that have been identified so far, the proteins in the insulin signaling pathway and p38 Mitogen Activated Protein Kinase (MAPK) pathway, which are signaling pathways involved in aging and stress tolerance, were analyzed in measure of oxidative stress tolerance, lifespan, and motility in the deficient mutants. Consequently, the phenotypes induced by BL were suppressed. These results suggested that BL caused the above bioactive effects through these signaling pathways. In addition to the previously revealed mechanism, I have further elucidated the mechanism.

Among the bioactive effects of bifidobacterium revealed in this study, the inhibition of age-related loss of motility and effects on muscle and mitochondria in *C. elegans* have not been reported to date. Although future studies in mice and other higher animals will be necessary, improving motility in aging individuals and maintaining muscle and mitochondrial function could prevent sarcopenia, a decline in muscle and motility with aging, and extend health span. Bifidobacterium intake may also develop into an inhibitory effect on Parkinson's disease (PD). PD is caused by aging and other factors and reduces mitochondrial homeostasis. Consequently, this causes dopaminergic neuronal degeneration. In the present study BL maintained the mitochondrial membrane potential in aging nematodes. This suggests that mitochondrial homeostasis is maintained and that

BL has the potential to prevent PD. In the future, I plan to analyze the effects of bifidobacterium on preventing sarcopenia and inhibiting PD.

Introduction

In modern society, human life expectancy is increasing compared to the past, and the average global life expectancy is now 73.2 years, compared to 47.0 years in the 1950s [1]. In recent years, the average life expectancy in Japan, a country known for its longevity, has been 85.0 years, and by the year 2100, the average life expectancy in Japan is expected to be 93.5 years [1]. In this society, the term “health span” is beginning to be used in addition to the term “life span”, which simply refers to the period from birth to death [2]. Health span is the period of time from birth to the time when a person is no longer able to perform healthy activities, i.e., until he or she becomes ill or bedridden and needs the assistance of someone else. Currently, health span in Japan is 72.14 years for men and 74.79 years for women [3]. Although there is a gap between the length of life span and health span, reducing the gap by extending health span is important to increase people's quality of life. Increasing health span includes having better medical care, maintaining good nutrition, and maintaining muscle mass through exercise. I focused on improving the body's health and anti-aging through food extracts and bioactive substances.

Bioactive substances are what can cause changes in our physiology and behavior when ingested. The classic study of phytochemicals (phytoalexins), which are functional components of plants, is resveratrol. Resveratrol is a kind of polyphenol found in red grapes and is known to be contained in red wine [4]. It is sometimes mythically attributed to the high intake of resveratrol that the French are healthy despite their fat-rich diet

(French Paradox) [5]. In fact, resveratrol has a strong antioxidant effect and various physiological effects such as atherosclerosis, heart disease, cerebral palsy, and metabolic disorders have been reported [6–9]. It is also known to have an effect on anti-aging and to extend life span in model organisms such as nematodes and yeast [10,11]. In the study on aging, an association between lifespan and sirtuin was suggested [12]. Sirtuin genes are histone deacetylases, which are involved in the silencing of transcription and repress gene expression [13]. Sirtuin genes and homologous genes are found in a wide range of organisms such as *C. elegans*, yeast, drosophila, and humans, with SIRT1~7 found in humans [14,15]. Sirtuin genes are also one of the genes so called longevity genes, and longevity genes are often included in several signaling pathways, which regulate aging by regulating the stress tolerance and energy expenditure of individuals [16]. For example, in *C. elegans*, Insulin/IGF-1 Signaling (IIS) pathway, p38 Mitogen-activated Protein Kinase (MAPK) pathway, Skinhead 1/NF-E2-Related Factor 2 (SKN-1/Nrf2) signaling pathway, c-Jun N-terminal Kinase (JNK) pathway, Heat Shock Factor 1 (HSF-1) pathway, and Target of Rapamycin (TOR) pathway are well known [17–24].

Signaling pathway

IIS pathway is activated by insulin-like peptides in DAF-2/IGF-1, receptor of peptides. Binding of antagonist peptides such as INS-1 to DAF-2 inactivates the IIS pathway, and the transcription factor DAF-16 is dephosphorylated and translocated to the nucleus, leading to stress tolerance [25]. DAF-16 is known to be homologous to mammalian

FOXO, which, as well as DAF-16, is a transcription factor involved in aging [26,27]. The transcription of DAF-16 extends the life span of nematodes. On the other hand, when an agonist peptide, such as DAF-28, binds to DAF-2, the transcription factor DAF-16 is phosphorylated via the IIS pathway and transferred to the cytoplasm, which represses its transcriptional activity [17,18,25]. p38 MAPK pathway is associated with defense against infection from bacteria [28]. This pathway is activated by Toll-like Receptor (TLR) when cells recognize foreign substances or are subjected to oxidative stress, and phosphorylates SKN-1/Nrf2 [29,30]. Phosphorylated SKN-1/Nrf2 migrates to the nucleus and acts as a transcription factor, regulating the transcription of various genes, thereby increasing the stress tolerance of individuals [20,31]. JNK pathway is also a kinase pathway and is activated by the some stressors. The transcription factor DAF-16 is activated via JKK-1 and JNK-1 in *C. elegans* when stimulated by environmental stress and other factors [22]. Subsequently, similar to IIS pathway, DAF-16 regulates the transcription of various senescence-related genes, resulting in phenotypes such as increased stress tolerance [32]. HSF-1 is a transcription factor that regulates the transcription of genes involved in heat stress, primarily in response to stress stimuli, and is involved in regulating lifespan [23]. Some transcriptions are also promoted by the co-localization of DAF-16 and HSF-1 in the nucleus [33]. TOR pathway is activated by rapamycin and nutrient stimuli. In this pathway LET-363 acts centrally. Activation of LET-363 shortens the lifespan by repressing transcription factors such as DAF-16, SKN-1, HSF-1, and PHA-4 [24,34]. It

is intricately related to various signaling pathways and therefore, there are many unexplored aspects.

This study focused on bifidobacterium, among other bioactive substances, to analyze their effects on health and anti-aging. In addition, *C. elegans* was used as an experimental model organism.

Bifidobacterium

Bifidobacterium is gram-positive rod bacteria [35]. It is also a partial anaerobic bacterium, which makes it difficult to grow in the presence of oxygen [36]. For this reason, bifidobacterium is more abundant in the human intestine, such as the large intestine, where it is even harder for oxygen to reach than in the stomach and duodenum [37]. Bifidobacterium such as *B. bifidum*, *B. infantis*, *B. breve*, *B. adolescentis*, *B. longum*, *B. angulatum*, and *B. catenulatum* are known to live in the human intestine [38,39]. Bifidobacterium is known as typical probiotics and is one of the intestinal bacteria that has a positive impact on humans [40]. Lactobacillus, a well-known probiotics, is a facultative anaerobe and can grow in the presence of oxygen and produce lactic acid as a metabolite [41]. Bifidobacterium, on the other hand, in addition to lactic acid, produce acetic acid, which lowers pH in the intestine and regulates the intestinal environment [42]. Bifidobacterium is the most predominant in the intestinal flora of human infancy. Later, although their numbers decrease in adults, they are 100-1,000 times more present than lactobacilli and are known to have the highest percentage of probiotics in the intestines

[43]. Due to its high proportion, it is likely to have considerable influence on the host. In fact, they are known to show beneficial effects on human health such as improving intestinal flora [44]. The anti-aging effects of probiotics were first reported in 1908 in Ilya Mechnikov's book "The prolongation of life" [45]. In his book, he noted that Bulgarians live long due to the constant consumption of probiotics, for example, intake of yogurt. Nowadays, various physiological effects of bifidobacterium are known, such as enhanced immune function and alleviation of allergies [46,47]. It has also been reported that bifidobacterium inhibits cancer development [48]. More recently, it has been reported that the stimulation of intestinal bacteria affects the brain, called gut-brain axis, and affects muscles, called gut-muscle axis, which greatly affects the host [49–51]. Although more than 100 years have passed since Ilya mechnikov's report, research on gut bacteria and aging has not progressed much, and there are still many unanswered questions, which I addressed in the present study [52].

Caenorhabditis elegans

C. elegans used as an experimental model organism in this study belongs to the phylum of molting animals and linear animals. Their epidermis are covered with a thick layer of cuticular, and it molts four times before becoming an adult [53]. In nature, nematodes live in soil and feed on bacteria by moving their pharynxes back and forth while advancing through the soil. They feed on *E. coli* at 20°C in the laboratory condition and survive for about a month on agar medium. They are easy to culture and can be observed with a 10x

optical microscope, so they do not require a sophisticated laboratory environment. They are also mostly hermaphroditic, so they can self-fertilize and lay eggs without mating [54,55]. They lay the next generation of eggs in 4 or 5 days after hatching from the eggs, so generation change is rapid. Because of the ease of rearing as mentioned above, *C. elegans* is widely used as a model organism for aging experiments. Similarly, the life span of mice, which are often used as experimental model organisms, is a few years, so nematodes are suitable for experiments to analyze aging due to their short life span [56]. It is also known that many of genes are homologous to those of higher animals [57]. In the early days, Sydney Brenner and his colleagues analyzed the cellular lineage and now the whole genome structure and whole cell genealogy have been revealed [58]. To their credit, there has been an abundance of research and a wealth of deletion mutants and recombinants created by numerous research groups. Many of them have been maintained in Caenorhabditis genetics center (CGC, University of Minnesota, Minneapolis, USA) and National BioResource Project (NBRP, Tokyo Women's Medical University, Tokyo, Japan), and have therefore been used as a model for specific neural and protein analysis [59,60]. *C. elegans* was the first organism for which RNA interference (RNAi) was established by AZFire and has since been studied using various genetic manipulation techniques, including genetic modification using CRISPR [61,62]. They also have basic intestinal, neural, and reproductive organs that allow them to mimic the digestion and absorption of food extracts and functional substances. In addition, the intestinal microbiota of *C. elegans* is important for present study. In the laboratory environment, as

well as this study, *C. elegans* are fed only *E. coli* from the egg state to grow, so it is likely that almost exclusively *E. coli* bacteria grow in the intestine. It is also known that there are dozens of types of intestinal bacteria in the wild [63,64]. Because of the above reasons, this method is often used to analyze the bioactive effects of substances. I have also used nematodes to measure the bioactive effects of phytochemicals, which are functional components of plants, food extracts and so on [65–69]. In recent years, public criticism of animal ethics has increased, and alternative biological model organisms are needed. *C. elegans* could be an alternative model organism because of the points mentioned above [70,71].

Previous studies of bifidobacterium using nematodes

Several previous studies have analyzed the bioactive effects of bifidobacterium using *C. elegans* [66,72–77]. Among the previous studies, there are only a few ones on senescence, including mine [66,73,75,77]. The cell wall components of bifidobacterium are said to be receptive to the nematodes, resulting in a bioactive effect [75]. Although there seems to be a difference in the signaling pathways activated by different species of bacteria, bifidobacterium activate IIS, TLR, p38 MAPK, and JNK pathways, extending their lifespan (Fig. 1) [78]. For example, *Bifidobacterium infantis*, which is a different species from the one I used, did not activate IIS pathway but activated p38 MAPK pathway, extending the life span of *C. elegans* [73]. In studies using *Bifidobacterium longum*, including my previous study, stimulation from IIS and JNK pathways activated the

transcription factor DAF-16 and regulated the transcription of various senescence-related genes, resulting in *B. longum* improving stress tolerance and extending life span [66,75]. Thus, despite the existence of several previous studies, there are still many unanswered questions regarding aging and life span. In addition, there may be bioactive effects of bifidobacterium on aging and health that are not yet clear. In this study, I aimed to explore the new bioactive effects of *B. longum* on aging and health by feeding sterilized *B. longum* (BR-108) together with *E. coli*, the food source for nematodes. Additionally, I aimed to elucidate the mechanism by using the genetic mutants mentioned above. The reason for using dead bacteria instead of live ones was that I wanted to use them for future applications in higher animals by oral ingestion, taking into account the possibility of bifidobacterium being killed by stomach acid. When considering future food applications, the use of dead bacteria rather than live ones will stabilize the quality. In addition, since substances with life-extending effects are said to be present in the cell wall fractions of bifidobacterium, it is thought that bioactive effects may exist even in dead bactericidal fractions [73,75]. A previous study using *Lactobacillus*, it has been reported that dead bacterial fractions are more readily accepted by nematodes and have a greater bioactive effect than live bacteria [79].

In this study, I aimed to explore the new bioactive effects of bifidobacterium on anti-aging, which have not been clarified so far, and aimed to elucidate the involved mechanism.

Materials and Methods

Nematodes, Bifidobacterium

C. elegans Bristol N2 wild type, SB1370[*daf-2*(e1370)III], TJ1052[*age-1*(hx546)II], RB754[*aak-2*(ok524)X], GR1307[*daf-16*(mgDf50)I], tm5464[*eat-2*(tm5464)II], PS3551[*hsf-1*(sy441)I], IG10[*tol-1*(nr2033)I], RB1085[*tir-1*(ok1052)III], tm850[*nsy-1*(tm850)II], AU1[*sek-1* (ag1)X], tm676[*pmk-1*(tm676)IV], tm4241[*skn-1*(tm4241)IV], RB1206[*rsks-1*(ok1255)III], VC1027[*daf-15*(ok1412)/nT1 IV; +/nT1 V], tm4642[*rheb-1*(tm4642)III], tm4598[*pha-4*(tm4598)V], TJ356[zIs356(*daf-16*p::*daf-16*a/b::GFP + *rol-6*)IV], LG333[geIs7(*skn-1*b::GFP)IV], RW1596[stEx30(*myo-3*p::GFP::*myo-3*+*rol-6*)V], SJ4103[zcIs14(*myo-3*::GFP(mit)). The above nematodes were obtained from CGC and NBRP. *C. elegans* was reared on Nematode Growth Medium (NGM) at 20℃ coated with *E. coli* OP50 strain (OP plates) [54,80].

Bifidobacterium longum (BR-108) (Combi Corporation, Tokyo, Japan), which was heat-sterilized at 105°C for 20 minutes. For storage, 500 mg/ml aqueous solution of BR-108 was stored frozen at -80°C. The frozen BR-108 aqueous solution was thawed and mixed with OP50 to a concentration of 50 mg/ml for the experiments. I made two samples; worms grown on OP plates (CT) and on BL plates which coated with a mixture of OP50 and *B. longum* (BL).

Synchronization

Adult nematodes were collected by S-basal (0.1 M NaCl (Kanto Chemical, Tokyo, Japan), 50 mM Potassium Phosphate Buffer (PPB (pH 6.0))). The adults were treated with NaClO solution (10 N NaOH (FUJIFILM Wako Pure Chemical Corporation, Osaka, Japan): NaClO (Haiter (Kao, Tokyo, Japan) = 1:10)). The nematodes were crushed by this treatment and the eggs were collected for the experiments. The L1 larvae obtained after incubating the collected eggs at 20°C for 18 hours were used for the experiments. The synchronization treatment was done to align the growth stage of the eggs used in the experiment.

Gene expression

Synchronized N2 wild-type nematodes were grown on OP plates for 96 hours and then transferred to OP or BL plates (day 0). After the synchronization treatment, 0.5 mg/ml FUdR (FUJIFILM Wako) was used at day -1 and 0 to inhibit egg laying and development. On the day 3, nematodes were collected and washed with dDW, and then crushed with Bio Masher II (Nippi, Tokyo, Japan) and Power Masher II (Nippi). mRNA was extracted from the crushed solution using RNAiso Plus (Takara Bio, Shiga, Japan). Subsequently, cDNA was synthesized using the cDNA reverse transcription kit PrimeScript™ RT reagent Kit with gDNA Eraser (Takara Bio). It was used to perform qPCR by THUNDERBIRD SYBR qPCR Mix (Toyobo, Osaka, Japan) and Thermal Cycler Dice® Real Time System Lite (Takara Bio). Based on previous study, I chose actin, *tba-1* and

Y45F10D4 on candidate genes for internal control [81]. From previous and present study, I chose Y45F10D4 as an internal control for the expression stability (Fig. 2) [81]. Each sample cDNA was measured in three wells. The primers used in this assay were shown in table 1.

Table 1 Sequences of primers used in the gene expression analysis

Gene name	5’-3’Sense	5’-3’Anti-sense
actin	TCGGTATGGGACAGAAGGAC	CATCCCAGTTGGTGACGATA
tba-1	TCAACACTGCCATCGCCGCC	TCCAAGCGAGACCAGGCATCAG
Y45F10D4*	CGACAACCCGCGAAATGTCGGA	CGGTTGCCAGGGAAGATGAGGC
hsp-12.6	TGGAGTTGTCAATGTCCTCG	GACTTCAATCTCTTTTGGGAGG
hsp-16.2	TGTTGGTGCAGTTGCTTCGAATC	TTCTCTTCGACGATTGCCTGTTG
hsp-70	ACCCTTCGTTGGATGGAACG	GCATCCGGAACCTGATTGGGC
sod-1	TGGTGGACCAAAATCCGAGA	CCATAGATCGGCCAACGACA
sod-2	GATACTGTCCAAAGGGAAAGAT	GTAGTAAGCGTGCTCCCAGA
sod-3	GCTGCAATCTACTGCTCGCACTG	GGCTGATTACAGGTTCCAAATCTGC
sod-4	GCACCAGATGACTCGAACA	GTCCACTTAATGAGGCAAGA
sod-5	TCGAAACGTGCTGTAGCGG	CACCTTCGGCTTTCTGGGT
ctl-1	CCAAACAGCCACCCAAATCA	AGTGTCGGCGTTCAGATTTC
ctl-2	CTGGGAGAAGGTGTTGGAT	GGATGAACCTTTGAAAAGTGAT
ctl-3	AGTAAATCTTCAAAATGCCAATG	GGTGGGGTTCCTGATTTCTAT
gst-4	CGTTTTCTATGGAAGTGACGC	TCAGCCCAAGTCAATGAGTC
gpx-1	AACGACTGATCCAAAGGAC	TTGAAAGTTTGAATTGCTG
gpx-2	GACTACTGAGCCGAAGGAT	CCAAGTTTTCACTCGATTTT
gpx-3	ATCTGGTAACATGGCACCT	TCCAACGCATTGTTTCATC
gpx-4	TACTTACTTTGGCTGTTTCTTTCAC	TTTCCAGCGCAGAGTATCG
gpx-5	TCGTAGTACCGACCCACAT	GTAAATACAGGAACGGAGAAAA
gpx-6	GCCAGATATGTATTCAAAGG	GCTGATAATGATGAGCCAC
gpx-7	GGCCATTGATTGGAGAAGA	CCATTTGATTGCATCGAAAA
gpx-8	TGGCGAATGAAACAGTAAA	GACAGTCGTTGATCTATGC
eat-3	CGACATCTGCTCAAACTTCGAT	CCAAGACCCATTTGAATCGAAC
fzo-1	GTGCTGCCGATAATGAACCAC	TTCCCGCTGTTCAGAACTAAC
drp-1	GAAGACGGTCAAATGGAACAC	GCACGGCATCGAAGTCTGT

*Reference gene.

UV stress tolerance assay

Nematodes are reduced in locomotion by UV stress. To measure their recovery from that decrease, synchronized N2 worms were grown on OP or BL plates for 96 hours, then the plates were placed in a UV irradiation machine (CL-1000, Analytik Jena AG, Jena, Germany) and subjected to UV-B and UV-C (100 mJ/cm^2) stress for 30s (hour 0), the number of thrashing motions of nematodes was measured for 15s in every 6 h. In this experiment, the motility of the nematodes at 20°C without UV exposure was measured simultaneously and calculated the difference between the number of locomotions with and without UV and presented the results. N=10, independent experiments were performed at least two times.

Heat stress tolerance assay (motility)

Heat stress reduces motility in nematodes. In order to measure their recovery from this loss of motility, synchronized N2 nematodes were grown on OP or BL plates for 96 hours and then exposed to heat stress at 35°C for 4 hours (hour 0), and the number of thrashing movements of nematodes was measured for 15s in every 6 hours. In this experiment, the motility of the nematodes at 20°C without heat exposure was also measured, and the results showed the motility recovery in terms of the difference between the motility of the nematodes at 35°C and the motility of the nematodes at 20°C. N=10, independent experiments were performed at least three times.

Heat stress tolerance assay (survival)

In order to measure the survival under heat stress, synchronized N2 nematodes were grown on OP or BL plates for 96 hours and then exposed to a heat stress environment at 35°C for 10 hours (hour 0) and the survival rate of N2 worms was measured in every 2 hours. Similar measurements were made for RB754 (*aak-2*), PS3551 (*hsf-1*), tm850 (*nsy-1*), AU1 (*sek-1*), and tm676 (*pmk-1*). N=40, independent experiments were performed at least two times.

Oxidative stress tolerance assay (hydrogen peroxide)

In order to measure the survival against hydrogen peroxide-induced oxidative stress, synchronized N2 nematodes were grown on OP or BL plates for 96 hours and then transferred to 0.3% hydrogen peroxide (Sigma-Aldrich, St. Louis, USA) (hour 0) and the survival rate of N2 nematodes was measured in every hour. 400 µl hydrogen peroxide was added to 24-well plates (Techno Plastic Products AG (TPP), Trasadingen, Switzerland). N=24, independent experiments were performed at least three times.

Oxidative stress tolerance assay (paraquat)

In order to measure the survival against oxidative stress caused by paraquat, synchronized N2 worms were grown on OP or BL plates for 96 hours and then transferred to 300 mM paraquat (Sigma-Aldrich) (hour 0) and the survival rate of N2 nematodes was measured in every hour. 400 µl paraquat was added to 24-well plates (TPP). Similar measurements

were performed for RB754(*aak-2*), GR1307(*daf-16*), IG10(*tol-1*), RB1085(*tir-1*), tm850(*nsy-1*), AU1(*sek-1*), tm676(*pmk-1*), tm4241(*skn-1*), RB1206(*rsks-1*). N=12, independent experiments were performed at least two times.

Nuclei localization of DAF-16

In order to observe the nuclei localization of DAF-16. Synchronized TJ356(*daf-16*::GFP) nematodes were grown on OP or BL plates for 96 hours. After washing the nematodes with S-basal, they are fixed with 10% ethanol (Kanto Chemical) for 10 min. GFP fluorescence was measured by the fluorescent microscope BZ8000 (Keyence, Osaka, Japan). N≥20, independent experiments were performed at least two times. The subcellular localization of fluorescence was classified into three groups: mainly localized to the nucleus (nuclei), partially localized to the nucleus (partial), and localized to the cytoplasm (cytoplasm), and the proportions were shown [82].

Intracellular ROS assay

Synchronized N2 nematodes were grown on OP or BL plates for 96 hours. After washing the nematodes with S-basal, 400 µl of DCF-DA solution was added and stirred for 1 hour. Then, after fixation with 10% ethanol (Kanto Chemical) for 10 min, the amount of intracellular ROS was measured by fluorescence microscope BZ8000 (Keyence). DCF-DA staining can measure intracellular ROS [83]. The DCF-DA solution was made by dilution of DCF-DA reagent (FUJIFILM Wako) to 100 mM with Dimethyl sulfoxide

(DMSO (FUJIFILM Wako)) and 50 μM with S-basal. N≥39, independent experiments were performed at least two times.

Life span assay

Synchronized N2 nematodes were grown on OP plates for 96 hours and then transferred to OP or BL plates (day 0). Thereafter, the plates were changed every 2 days and the survival rate of N2 nematodes was measured. Survival was determined by nematode movements by gentle contact stimulation using a platinum picker. On the day -1, 0, 2, and 4, 0.5 mg/ml 2'-Deoxy-5-fluorouridine (FUdR (FUJIFILM Wako)) was used to suppress egg laying and development [84]. FUdR was dissolved in dDW at 5.0 mg/ml and stored frozen at -80°C. It was diluted to 0.5 mg/ml in S-basal and used for the treatment. Similar measurements were performed for RB754(*aak-2*), PS3551(*hsf-1*), IG10(*tol-1*), RB1085*(tir-1*), tm850(*nsy-1*), AU1(*sek-1*), and tm676(*pmk-1*). N=60, independent experiments were performed at least two times.

Egg laying

Synchronized N2 nematodes were grown on OP or BL plates for 48 hours and then transferred to new OP or BL plates (day 0). Thereafter, the plates were changed every day and the number of eggs was measured. N=10, independent experiments were performed at least twice.

Food intake

Synchronized N2 nematodes were grown on OP plates for 96 hours and then transferred

to OP or BL plates (day 0). Thereafter, the plates were changed every 3 days and the number of pumping rate of N2 wild-type was measured for 15s. *C. elegans* intakes food simultaneously with pharyngeal movements [85]. On the day -1, 0, and 3, 0.5 mg/ml FUdR (FUJIFILM Wako) was used to inhibit egg laying and development. N=10, independent experiments were performed at least twice.

Long-term motility assay

Synchronized N2 nematodes were grown on OP plates for 96 hours and then transferred to OP or BL plates (day 0). Thereafter, the plates were changed every 3 days and the number of thrashing movements of N2 nematodes was measured for 15s. On the day -1, 0, and 3, 0.5 mg/ml FUdR (FUJIFILM Wako) was used to inhibit egg laying and development. N=10, independent experiments were performed at least three times. Similarly, measurements were performed for RB754(*aak-2*) and PS3551(*hsf-1*) until day 9. To examine the association with mitochondria the same experiments were conducted with the inhibitors of the mitochondrial complex I, II, III, IV and V: rotenone (Sigma-Aldrich), 2-thenoyltrifluoroacetone (TTFA, Sigma-Aldrich), antimycin A (Sigma-Aldrich), sodium azide (FUJIFILM Wako) and N,N-dicyclohexylcarbodiimide (DCCD, FUJIFILM Wako) respectively. 10-, 20-, and 50 µM rotenone, 500-, 1,000, 2,000 µM TTFA, 1-, 10-, and 20 µM antimycin, 100-, 200-, and 400 µM sodium azide, and 20-, 50-, and 100 µM DCCD were dropped into the plate at the same time as the plate change. N=10, independent experiments were performed at least two times.

Fat accumulation

Synchronized N2 wild-type nematodes were grown on OP or BL plates for 96 hours. Thereafter, they were fixed with 4% paraformaldehyde (FUJIFILM Wako) for 2 hours at 4°C. After washing with S-basal, 400 µl of 5 µg/ml Nile Red staining solution (FUJIFILM Wako) was added and the samples were stirred for 10 min at 4 °C. The mixtures were washed twice with S-basal again and measured by a fluorescence microscope BZ8000 (Keyence). N≥26, independent experiments were performed at least three times.

Long-term muscle mass assay

Synchronized nematodes RW1596(*myo-3*::GFP) were grown on OP plates for 96 hours and then transferred to OP or BL plates (day 0). Thereafter, the plates were changed every 3 days and GFP fluorescence was measured with a fluorescent microscope BZ-X810 (KEYENCE). As well as motility measurements, spawning and development were inhibited with 0.5 mg/ml FUdR (FUJIFILM Wako) at day -1, 0, and 3. N≥13, independent experiments were performed at least three times.

Long-term intramuscular mitochondrial mass

Synchronized nematodes SJ4103(*myo-3*::GFP(mit)) were grown on OP plates for 96 hours and then transferred to OP or BL plates (day 0). Thereafter, the plates were changed every 3 days and GFP fluorescence was measured with a fluorescent microscope BZ-X810 (KEYENCE). As well as motility measurements, spawning and development were

inhibited with 0.5 mg/ml FUdR (FUJIFILM Wako) at days -1, 0, and 3. N≥11, independent experiments were performed at least three times.

Mitochondrial homeostasis assay

Synchronized nematodes (SJ4103(*myo-3*::GFP(mit))) were grown on OP plates for 96 h and then transferred to OP or BL plates (day 0). Thereafter, the plates were changed every 3 days and observed with a fluorescent microscope THUNDER imaging system (Leica, Wetzlar, Germany). Spawning and development were suppressed using 0.5 mg/ml FUdR (FUJIFILM Wako) at days -1, 0, and 3 as well as motility measurements. N≥5, independent experiments were performed at least two times.

ATP assay

Synchronized N2 nematodes were grown on OP plates for 96 hours and then transferred to OP or BL plates (day 0). On the day -1, 0, and 3, as well as motility measurements, 0.5 mg/ml FUdR (FUJIFILM Wako) was used to inhibit spawning and development. More than 200 nematodes were collected and washed with MilliQ, and then crashed with Bio Masher II (Nippi, Tokyo, Japan) and Power Masher II (Nippi) every 3 days. The crushed fluid was cooled and centrifuged (4°C, 1,000 g, 10 min.) and ATP was extracted using the "Tissue" ATP assay kit (TOYO B-Net Co., Ltd., Tokyo, Japan). Luciferase luminescence was then quantified using a white 96-well plate (FUJIFILM Wako) and a

luminometer (Berthold Technologies, Bad Wildbad, Germany). Each sample ATP was measured in three wells. Independent experiments were performed at least two times.

Long-term mitochondrial membrane potential and mitochondrial ROS assay

Synchronized nematodes SJ4103(*myo-3*::GFP(mit)) were grown on OP plates for 96 hours and then transferred to OP or BL plates (day 0). Thereafter, the plates were changed every 3 days. In order to measure mitochondrial membrane potential and mitochondrial ROS, 1 ml of 0.5 μM MitoTracker Orange CMTMRos (Thermo Fisher Scientific, Inc., Waltham, USA) and 1 ml of 0.5 μM MitoTracker Orange CM-H2TMRos (Thermo Fisher Scientific) were added respectively. 3 hours later, the samples were collected and washed. Thereafter, nematodes were fixed in 10% ethanol (Kanto Chemical) for 10 mins and the fluorescence of MitoTracker was measured by BZ-X810 (KEYENCE). As well as motility measurements, spawning and development were inhibited with 0.5 mg/ml FUdR (FUJIFILM Wako) at day -1, 0, and 3. N≥13, independent experiments were performed at least three times. Same experiments were conducted with the inhibitors of the mitochondrial complex: rotenone (Sigma-Aldrich), 2-thenoyltrifluoroacetone (TTFA, Sigma-Aldrich), antimycin A (Sigma-Aldrich), sodium azide (FUJIFILM Wako) and N,N-dicyclohexylcarbodiimide (DCCD, FUJIFILM Wako) respectively. 10-, 20-, and 50 μM rotenone, 500-, 1,000, 2,000 μM TTFA, 1-, 10-, and 20 μM antimycin, 100-, 200-, and 400 μM sodium azide, and 20-, 50-, and 100 μM DCCD were dropped into the plate at the same time as the plate change. For membrane potential assay, N≥13 for vehicle,

≥13 for rotenone, ≥13 for TTFA, ≥11 for antimycin A, ≥10 for sodium azide, ≥10 for DCCD. For mitochondrial ROS assay, N≥11. independent experiments were performed at least two times.

Statistical analysis and figure drawing

Statistical analysis and figure drawing were conducted by Python (ver. 3.6.9, Python Software Foundation, Delaware, USA) on Google colaboratory (Google LLC, California, USA, https://colab.research.google.com/) with the following packages: matplotlib, scipy, statsmodels and lifelines. Data were presented as the mean ± SEM, and statistical analysis was performed using *Student's t-test* for the two-group test, and one way ANOVA followed by *Tukey's HSD* post hoc test for the three or more group tests. The survival rate was drawn using *Kaplan-Meier* curve and analyzed using *log-rank test*. P value < 0.05 was considered to indicate statistical significance.

Results

The purpose of this study was to explore the new bioactive effects of *B. longum* (BL, BR-108) on anti-aging and health and to elucidate the mechanism. First, I measured the stress tolerance of *C. elegans* after the consumption of BL. Stress tolerance is closely related to anti-aging and lifespan. Stress on cells leads to the production of ROS and protein aggregation. Consequently, these reduced cell homeostasis and accelerated aging [86]. In other words, increased stress tolerance can be expected to increase anti-aging and lifespan [87–89]. In the present study, UV, hydrogen peroxide, paraquat and heat at 35°C were chosen as the stress sources. First, nematodes were irradiated with 100 mJ/cm^2 UV-A, but the results were not stable. Then I measured the motility of the nematodes at 0, 6, and 12 h after irradiation with UV-B and at 0 and 6 h after irradiation with UV-C. Consequently, the motility of the nematodes decreased after UV irradiation. I measured the differences in motility between the nematodes with and without irradiation, and found that the motility of the nematodes treated with BL increased at each hour after UV-B and UV-C irradiation, suggesting that BL enhanced their recovery from UV stress (Fig. 3A,B). The increase in motility even at 0 h after UV irradiation suggested that BL provided a protective function for *C. elegans* against UV radiation.

In N2 wild-type nematodes, BL enhanced the motility after 4 h of heat stress at 35°C, the survival under continuous 35°C heat stress, and the survival to 300 mM paraquat and 0.3% hydrogen peroxide (Fig. 4-8). This suggests that BL enhanced the heat stress and

oxidative stress tolerance of *C. elegans*. To investigate which signaling pathway is responsible for these increased stress tolerances, I used several gene deficient mutants. Increased survival under heat stress was not observed in RB754(*aak-2*), PS3551(*hsf-1*), tm850(*nsy-1*), AU1(*sek-1*) and tm676(*pmk-1*) (Fig. 5B-F). Increased oxidative stress tolerance using paraquat was not observed in RB754(*aak-2*), GR1307(*daf-16*), RB1085(*tir-1*), tm850(*nsy-1*), AU1(*sek-1*), tm676(*pmk-1*), tm4241(*skn-1*), RB1206(*rsks-1*), VC1027(*daf-15*) and tm4642(*rheb-1*) (Fig. 7A-H,8A-C). Therefore, it is suggested that the enhancement of heat and oxidative stress tolerance is mediated by these pathways. In order to further investigate the signaling pathways involved in stress tolerance, I measured the nuclei localization of the transcription factor DAF-16. The worms fed on BL had more bright dots compared with CT (Fig. 9A,B). The same can be seen from images observed under high magnification (Fig. 9C,D). It suggested BL induced the nuclei localization of DAF-16 (Fig. 9E). This localization might result in the increase of stress tolerance [25]. Various stresses generate ROS and damage cells [90–92]. I used DCF-DA to analyze whether BL changes the amount of ROS in cells. Compared to CT, the amount of fluorescence was lower in BL (Fig. 10A,B). The results showed that BL significantly decreased ROS in *C. elegans* (Fig.10C). It is suggested that this decline of ROS resulted in an increase of stress tolerance. The result of gene expression that BL upregulated some genes related to heat stress tolerance, HSPs, and oxidative stress tolerance and removal of ROS, SODs, CTLs, GPXs and GST-4 also contribute to this upregulation of stress tolerance (Fig. 11).

As mentioned earlier, increased stress tolerance, ROS generation, and lifespan extension are closely related [93]. BL extended the lifespan of wild-type *C. elegans* (Fig. 12A). In order to analyze whether this BL-induced life span extension was due to the effect on ROS reduction and stress tolerance enhancement or due to caloric restriction, I measured egg laying and food intake. Consequently, BL did not change the number of eggs and amount of food intake (Fig. 13,14). This suggested BL-induced extension might be due to the reduction of ROS and increased stress tolerance [66,78]. To further elucidate the known mechanism of life span extension by *B. longum*, I used several gene deletion mutants and found that there was life span extension in PS3551(*hsf-1*) and IG10(*tol-1*), and no extension in RB754(*aak-2*), RB1085(*tir-1*), tm850(*nsy-1*), and AU1(*sek-1*) and tm676(*pmk-1*) (Fig. 12B-I). Thus, this suggested the lifespan extension was mediated by AAK-2, TIR-1, NSY-1 SEK-1 and PMK-1. To analyze the effects of life span as well as the health span of *C. elegans*, I analyzed the age-related motility retardation of nematodes. I found that BL fed wild-type nematodes maintained high motility in aged worms, indicating that BL prevented the decline in motility associated with aging (Fig. 15A). To examine the relationship between this mobility and health, I measured the fat mass in nematodes. BL decreased the fat accumulation significantly (Fig. 16). For further investigation, I used several gene deficient mutants and found that RB754 (*aak-2*) and PS3551 (*hsf-1*) did not show the upregulation of motility, suggesting that this upregulation was mediated by these pathway (Fig. 15B,C). It is possible that ROS generation and stress tolerance are also related to this improvement in motility, but the

question remains whether it changes that much [94]. Therefore, I analyzed the effects of BL on muscle and mitochondria, assuming that muscle and mitochondria are involved in the improvement of motility.

To analyze the effects of BL on muscle and mitochondria, I first quantified the muscle mass of RW1596 nematodes, in which GFP fused with *myo-3* in muscle. I found that the amount of fluorescence in RW1596 nematodes fed BL was significantly increased at day 3 and 6 compared to CT (Fig. 17C). This increase was observed especially at day 3 (Fig. 17A,B). This suggested that BL increased the muscle mass of nematodes. I next quantified the mitochondrial mass of SJ4103 nematodes, in which GFP fused with *myo-3* of mitochondria in muscle. I found that the amount of fluorescence in SJ4103 nematodes fed BL increased significantly at day 3, 6, 9, and 12 compared to CT (Fig. 18E). This increase was observed especially at day 9 (Fig. 18A,B). This suggests that BL maintained the number of mitochondria, which decreases with aging. To measure mitochondrial homeostasis, I also observed SJ4103 with a fluorescent microscope THUNDER imaging system (Leica). Normally, mitochondria in muscle are arranged in a line along the muscle fibers, but with aging, aggregation and tears occur and their arrangement becomes disrupted [95,96]. The results are displayed in the day 9 images, which were particularly strikingly observable (Fig. 18 C,D). Compared to the aged CT at day 9, the mitochondria were neatly placed on the line in the BL fed nematode. This suggests that BL not only inhibited the loss of mitochondria associated with aging in nematodes, but also

maintained homeostasis. Gene expression of mRNA involved in fusion and fission of mitochondrial was examined. Although the expression of *drp-1* related to mitochondrial fission was not changed, the expression of *eat-3* and *fzo-1* related to mitochondrial fusion was upregulated, though *fzo-1* no significance ($p = 0.051$) (Fig. 11) [97].

Mitochondria produce ATP for muscle energy, but with aging, homeostasis is lost and the ability to produce ATP decreases [98]. I measured ATP levels in nematodes and found significantly higher ATP in worms fed BL compared to CT at day 9, 12 and 15 (Fig. 19).

From the results shown above, I hypothesized that BL has a greater effect on mitochondria than on muscle and proceeded with the study. Therefore, I measured the mitochondrial membrane potential, an indicator of mitochondrial activity and found that it was substantially increased in nematodes given BL compared to CT (Fig. 20C). This increase was also observed in the aged worms at day 9 (Fig. 20A,B). In addition, mitochondria are one of the main cellular organelles that produce ROS. Therefore, I measured mitochondrial ROS longitudinally and found it was elevated in nematodes fed BL compared to CT (Fig. 21C). This increase was also observed in the aged worms at day 9 (Fig. 21A,B).

I confirmed that BL has a significant effect on mitochondria. Next, I aimed to investigate which complexes of mitochondria were affected by BL. Mitochondria have five complexes, I, II, III, IV and V, and I used the inhibitors rotenone, thenoyltrifluoroacetone (TTFA), antimycin A, sodium azide, and dicyclohexylcarbodiimide (DCCD) for each of

these complexes for the age-related motility assay [99–101]. The results showed a similar trend towards inhibitors of rotenone, TTFA, antimycin A, sodium azide and DCCD (Fig. 22). The addition of the inhibitors decreased motility in CT and BL nematodes, but the rate of decrease was either not significantly different or decreased compared to those without inhibitors (Fig. 22). This suggests that the increase in motility with aging is related to these complexes. Secondly, the mitochondrial membrane potential was measured using the aforementioned complexes. I found that only when the inhibitor of complex I was added, the BL-induced upregulation of mitochondrial membrane potential was decreased with the concentration of the inhibitor (Fig. 23A). When other inhibitors of complexes II, III, IV and V were used, there was no decrease in the mitochondrial membrane potential increased by BL (Fig. 23B-E), indicating that the increase of mitochondrial membrane potential caused by BL is mediated by complex I.

Discussion

The purpose of this study is to analyze the bioactive effects of bifidobacterium on health and anti-aging using C. elegans. C. elegans has a basic intestine, but since it is grown with only E. coli from the egg state, it is thought that almost only E. coli bacteria are present in the intestinal bacteria of C. elegans. Even in wild nematodes, less than 100 species of intestinal bacteria have been reported, which are far fewer than in humans and mice [102]. This made me think that it is more suitable for the analysis of a single BL bacterium rather than the interaction of intestinal bacteria. In the present study, I performed a "life span" related analysis and a "health span" related analysis. In relation to life span, I measured UV, heat and oxidative stress resistance, intracellular ROS, and life span. In relation to health span, I measured long-term motility, muscle mass, mitochondrial mass, mitochondrial membrane potential, and mitochondrial ROS. Furthermore, I hypothesized that BL has a significant effect on mitochondria with respect to motility, and I used an inhibitor of the mitochondrial complex. Previous studies that analyzed the bioactive effects of bifidobacterium using C. elegans have reported that the cell wall components of bifidobacterium increased stress tolerance via TLR in C. elegans, extending lifespan and resulting in immune-enhancing effects [29,77]. Based on studies in cultured cells and mice, TLR are thought to recognize the peptidoglycan layer and lipoteichoic acid of bacteria [103,104]. This suggests that BL used in this study also resulted in various bioactive effects via TLR. Stimulation from TLR activates the p38 MAPK pathway and

promotes the activation of SKN-1, which is involved in the transcription of genes related to stress tolerance [29–31]. In the present study, oxidative stress tolerance and life span were also increased via TIR-1 contained in TLR (Fig. 7H,12E). In addition, heat stress and oxidative stress and life span were increased via NSY-1, SEK-1, and PMK-1 in p38 MAPK (Fig. 5D-F,7C-E,12F-H), and life span and oxidative stress tolerance were increased via SKN-1 (Fig. 7F,12I). However, there was no TOL-1-mediated increase in oxidative stress tolerance or lifespan extension in TLR (Fig. 7G,12D); previous studies using B. infantis showed a TOL-1-mediated bioactive effect, while previous studies using B. longum were unknown for TOL-1, but JNK pathway was activated by the stimulation via TIR-1 [75,77]. Considering that different pathways are activated by different species of bacteria, it is possible that the bioactivity of B. longum was not mediated by TOL-1 but was mediated by TIR-1. A previous study using B. infantis did not show any activation of IIS pathway, whereas a study using B. longum appeared to show the activation of this pathway [66,73]. This pathway may also be involved in the bioactivity of BL, as the BL used in the present study also showed nuclei localization of DAF-16 (Fig. 9E). TIR-1 and DAF-16 were activated in BR-108 used in this study, as in previous studies of B. longum [75]. This suggests that the phenotype revealed in this study was not unique to the strain BR-108, but may be common to B. longum.

The stress tolerance of nematodes was increased by BL. Initially, BL increased UV stress tolerance, which can lead to DNA damage and senescence of individuals [105,106]. UV-

A, UV-B, and UV-C fall from the sun onto the earth; UV-C is absorbed by the earth's ozone layer and rarely reaches the ground, but has the highest level of energy; UV-B causes the most damage to nuclei DNA compared to other UV-A and UV-C [107]. UV-A has lower energy but longer wavelengths and higher penetration, so it reaches the dermis and accelerates the aging of the skin [108]. In this study, motility recovery was measured by irradiating nematodes with UV-A, UV-B, and UV-C. In present study, UV-B and UV-C were used to analyze the stress tolerance. That's because UV-A was not able to reduce motility of nematodes sufficiently, perhaps because of its low energy content. As a result, the motility of nematodes was significantly restored by BL compared to CT for both UV-B and UV-C (Fig. 3). Since UV stress tolerance is upregulated through p38 MAPK, SKN-1, and DAF-16, it is possible that BL increased the UV stress tolerance of C. elegans via these signals in this study as well [87,109].

BL increased the heat stress tolerance of C. elegans (Fig. 4,5). In the present study, I set up a short heat treatment for 4 hours to analyze the recovery from heat stress and a long heat treatment to analyze the resistance to heat stress. It is known that short heat treatment for C. elegans causes calcium efflux, damaging mitochondria and affecting motility [110]. Since BL increased the motility after heat exposure, BL might protect mitochondria and cause the increase of motility. In addition, long-time exposure of heat stress causes nematodes to accumulate a large amount of ROS [111]. Given the result of ROS measurement, what BL decreased ROS production suggested the increase of their

tolerance to heat stress. In present study the bioactive effect by BL was through DAF-16 (Fig. 7B,9E). Since DAF-16 is also involved in the increase in heat stress and colocalization of DAF-16 and HSF-1 upregulate the expression of genes related to heat stress tolerance such as hsp-12.6, hsp16.2 and hsp-70, increased in present study (Fig. 11) [33,112]. The activation of DAF-16 and HSF-1 by BL could be one of the causes of the increase in heat stress

BL increased oxidative stress tolerance. In this study, I measured the survival rate of wild-type C. elegans using hydrogen peroxide and paraquat as sources of oxidative stress (Fig. 6,7). Both hydrogen peroxide and paraquat produce ROS, but hydrogen peroxide produces H2O2 as ROS and paraquat produces superoxide anion (O2-) as ROS [113,114]. The generated O2- is detoxified by super oxide dismutase (SOD), which is decomposed to H2O2 and further decomposed to water by catalase [115,116]. In the present study, gene expression of SOD and catalase (CTL) was upregulated by BL, suggesting increased resistance to hydrogen peroxide and paraquat (Fig. 11). From the result of gene expression, GST-4 and some GPXs were also upregulated (Fig. 11). They upregulate by the nuclei localization of SKN-1 [116,117]. In this study it was suggested the bioactive effects of BL was through SKN-1 (Fig. 7F,12I). This can also explain the increase in stress tolerance.

In this study, in addition to the elucidated signaling pathways activated by BL previously, I also aimed to explore new pathways. Specifically, I used AAK-2, which acts as an AMPK, HSF-1, a transcription factor mainly involved in heat stress, and RSKS-1, DAF-

15, and RHEB-1, which are involved in TOR signaling [24,118]. aak-2 and hsf-1 mutants were used in the experiments, and the results showed that BL-induced upregulation of heat stress tolerance, and maintained motility was suppressed (Fig. 5B,C,15B,C). In addition, experiments with aak-2 mutants did not alter oxidative stress tolerance and life span (Fig. 7D,12B), suggesting that AAK-2 and HSF-1 may be responsible for the bioactive effects of BL. Additionally, the oxidative stress tolerance was not increased by BL in rsks-1, daf-15 and rheb-1 mutants (Fig. 8A,B,C). These results suggested that TOR signaling was possibly involved in the increase in oxidative stress tolerance in BL. TOR signaling is known to have a complex effect on various signals [34,119,120]. There are several reasons to activate TOR signaling, one of which is caloric restriction. The fact that, in the present study, the number of eggs laid and the amount of food ingested did not change in nematodes with and without BL suggests that the BL-fed nematodes were not calorie-limited (Fig. 13,14) [121]. Another cause is that stimulation from IIS pathway activates TOR signaling [34,120,122]. Since the bioactive effects of BL were mediated by IIS pathway in the present study, it is possible that the activation of TOR signaling by BL is derived from IIS pathway. It is very possible that other signaling pathways are also involved in the bioactive effects of BL. In the future, I will identify the involved signaling pathways by comprehensive analysis, such as RNA sequencing.

BL inhibited the decline in motility associated with aging in C. elegans and affected muscles and mitochondria. This inhibitory effect has the potential to prevent sarcopenia.

Sarcopenia is a symptom of the loss of muscle function with aging and causes movement disorders and other problems [123]. Currently, preventing sarcopenia includes good nutrition and exercise [124,125]. Since BL inhibited the decline in muscle function with aging, supplemental intake of BL has the potential to prevent this sarcopenia. In addition, as a side aspect, the increased motility of nematodes may have resulted in the consumption of fat as a substrate in the C. elegans body, since BL decreased the fat accumulation (Fig. 16) [126,127]. In the present study, I also focused on the mitochondrial complex to elucidate the mechanism of action of BL on mitochondria. Mitochondria have five complexes, complex I, II, III and IV involved in the electron transfer chain and complex V involved in the oxidative phosphorylation synthesis of ATP [128–130]. The inhibitors of each of the mitochondrial complexes, rotenone, TTFA, antimycin A, sodium azide and DCCD, were used. The concentrations were based on the ones that could cause a decrease in ATP of C. elegans in the previous study [131]. Consequently, the results of senescence motility did not lead to the identification of the specific complexes involved (Fig. 22). However, the mitochondrial membrane potential measurements suggested a strong involvement of complex I (Fig. 23A). Previous reports said that the mitochondrial complexes might not work individually, but rather by several complexes that aggregate and make the structure of a supercomplex [132–134]. Therefore, I considered the possibility that the bioactive action of BL through the mitochondrial complexes could be central to complex I, although all complexes work. Rotenone, the inhibitor of the mitochondrial complex I used in this study, is a known Parkinson's

disease-causing agent [135–137]. Parkinson's disease (PD) is designated as an incurable disease that causes tremors and strength in muscles throughout the body and interferes with daily life [138]. Dopaminergic neuronal degeneration due to mitochondrial dysfunction has been proposed as one of the causes [139–141]. A previous study has shown that the amount of bifidobacterium in the gut is significantly reduced in a PD model mouse [142]. The reduced bifidobacterium in the gut may trigger PD by decreasing mitochondrial function and causing degeneration of dopaminergic neuron. A study using the PD model drosophila has shown that restoring mitochondrial function and increasing membrane potential inhibited the development of PD [143]. I hypothesized that increasing the mitochondrial membrane potential by bifidobacterium might lead to the suppression of PD. In the future, I would like to analyze the inhibitory effect of BL on PD by giving BL to C. elegans overexpressing α-synuclein, which is said to cause PD by abnormal aggregation, and analyzing its effects on muscle [144–146]. It has also been reported that DAF-16 and AMPK, which were involved in the bioactive effects of BL, are related to muscle biosynthesis and mitochondrial homeostasis [96,147]. Therefore, it is possible that BL used in this study may also have a preventive effect on PD through these pathways.

In the future, I hope that quality of life will be enhanced by the generation and distribution of foods containing bifidobacterium that claim the functionalities revealed in this study.

Figures

Fig. 1 Signaling pathway

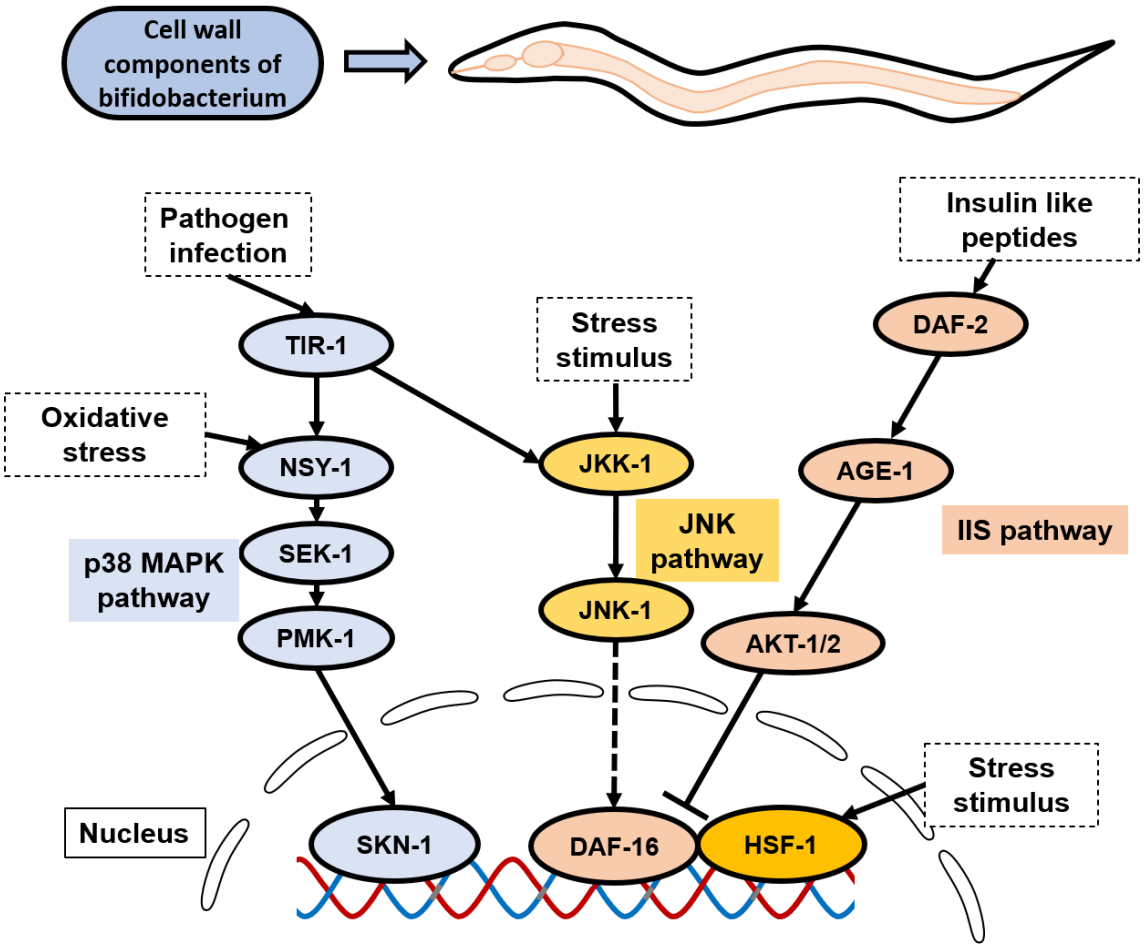

Fig. 1 Signaling pathway activated by bifidobacterium.

Previous studies have shown that bifidobacterium improves stress tolerance in C. elegans via several signaling pathways, causing anti-aging and longevity [66,72–78].

Fig. 2 Gene expression of internal control

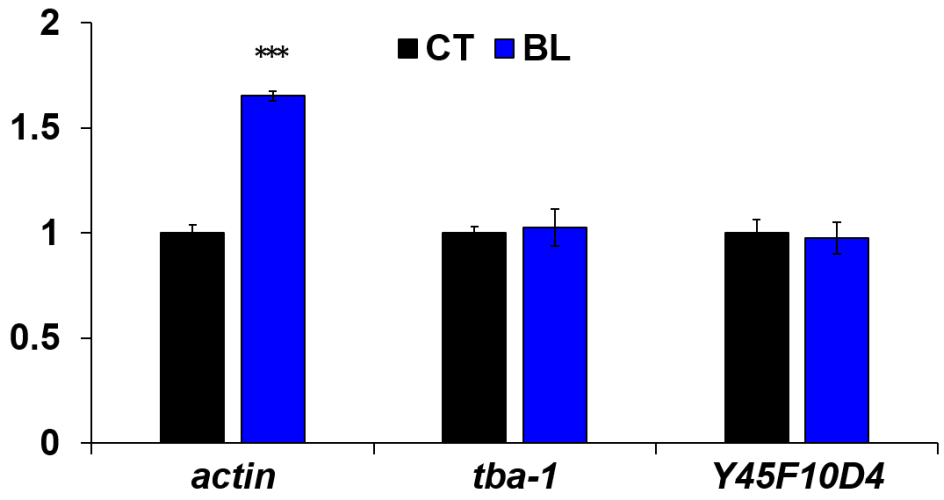

Fig. 2 Y45F10D4 was the most suitable for internal control.

Synchronized N2 wild-type nematodes were grown on OP plates for 96 hours and then transferred to OP or BL plates (day 0). After the synchronization treatment, 0.5 mg/ml FUdR was used at day -1 and 0 to inhibit egg laying and development. On the day 3, nematodes were collected and washed with dDW, and then crushed with Bio Masher II and Power Masher II. mRNA was extracted from the crushed solution using RNAiso Plus. Subsequently, cDNA was synthesized using the cDNA reverse transcription kit PrimeScript™ RT reagent Kit with gDNA Eraser. It was used to perform qPCR by THUNDERBIRD SYBR qPCR Mix and Thermal Cycler Dice® Real Time System Lite.

Each sample mRNA was measured in three wells. Data were presented as the mean ± SEM, and ***P < 0.005 according to the conducted *Student's t-test*.

Fig. 3 UV stress

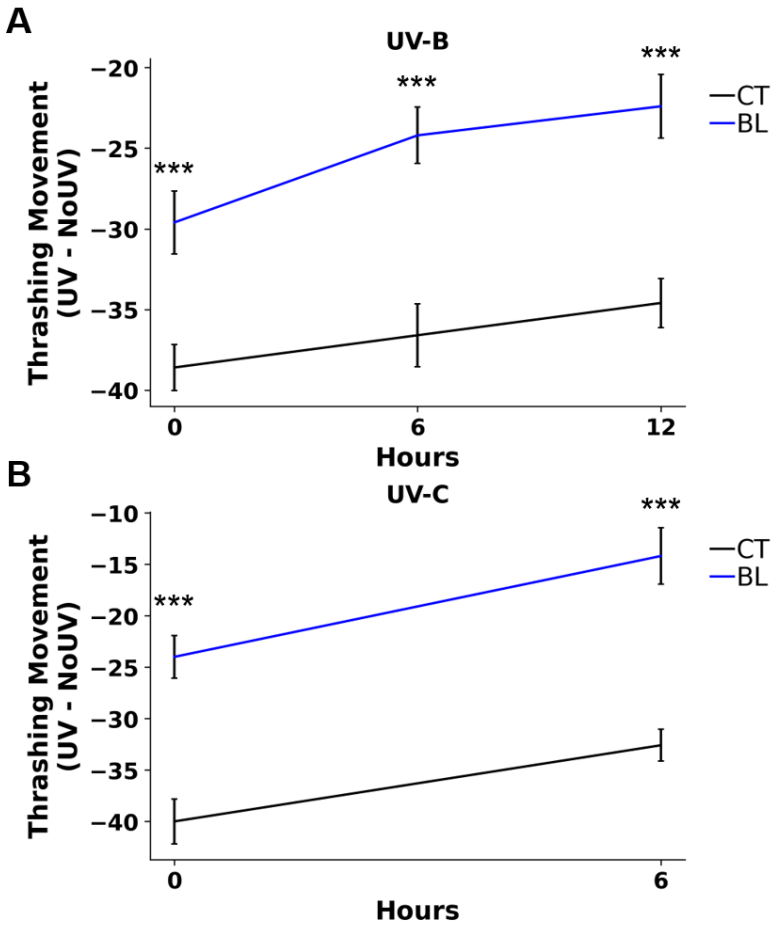

Fig. 3 BL increased UV stress tolerance.

Synchronized N2 worms were grown on OP or BL plates for 96 hours, then the plates were placed in a UV irradiation machine and subjected to UV-B and UV-C (100 mJ/cm^2) stress for 30s (hour 0), the number of thrashing motions of nematodes was measured for 15s in every 6 h. In this experiment, the motility of the nematodes at 20°C without UV

exposure was measured simultaneously and calculated the difference between the number of locomotions with and without UV and presented the results. Recovery of motility every 6 hours after (A) UV-B and (B) UV-C irradiation. N=10. Data were presented as the mean ± SEM, and ***P < 0.005 (vs CT at the same time period) according to the conducted *Student's t-test*.

Fig. 4 Heat stress (motility)

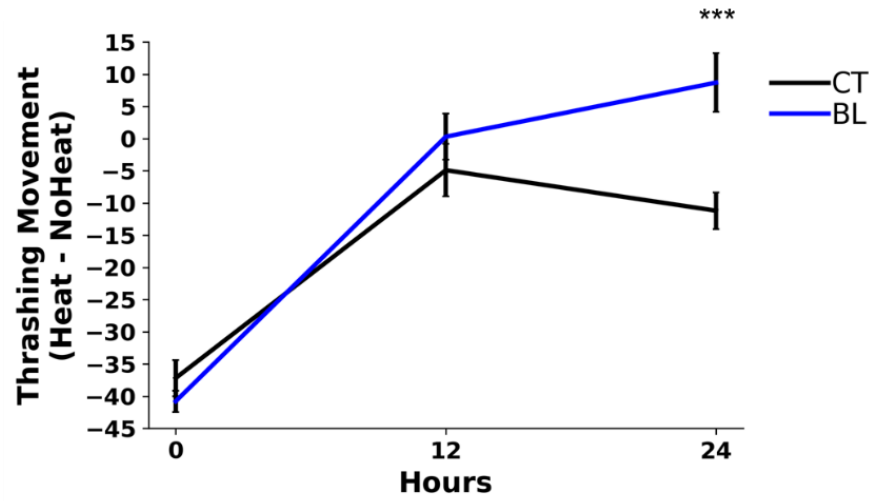

Fig. 4 BL increased the tolerance to short-time heat stress (motility).

Synchronized N2 nematodes were grown on OP or BL plates for 96 hours and then exposed to heat stress at 35°C for 4 hours (hour 0), and the number of thrashing movements of nematodes was measured for 15s in every 6 hours. In this experiment, the motility of the nematodes at 20°C without heat exposure was also measured, and the results showed the motility recovery in terms of the difference between the motility of the nematodes at 35°C and the motility of the nematodes at 20°C. N=10. Data were presented as the mean ± SEM, and ***P < 0.005 (vs CT at the same time period) according to the conducted *Student's t-test*.

Fig. 5 Heat stress (survival)

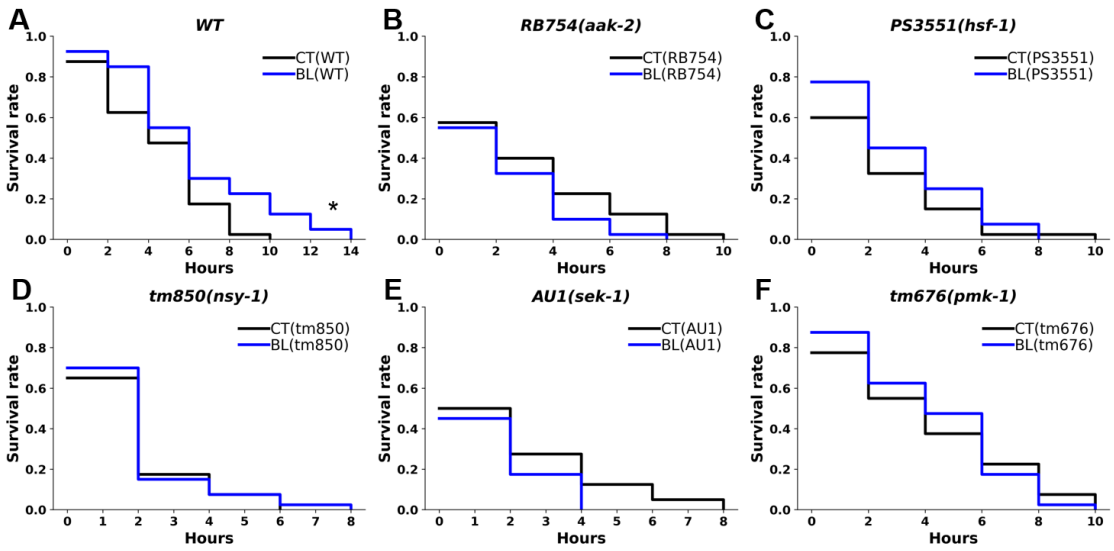

Fig. 5 BL increased the tolerance to long-time heat stress (survival).

Synchronized nematodes were grown on OP or BL plates for 96 hours and then exposed to a heat stress environment at 35°C for 10 hours (hour 0) and the survival rate of N2 worms was measured in every 2 hours. Survival rate of (A) N2 wild-type, (B) RB754, (C) PS3551, (D) tm850, (E) AU1 and (F) tm676 in 35°C condition after 10 hours of heat stress at 35°C. N=40. Data were presented as the *Kaplan-Meier* curve, and *P < 0.05 according to the conducted *log-rank test*.

Fig. 6 Oxidative stress tolerance (hydrogen peroxide)

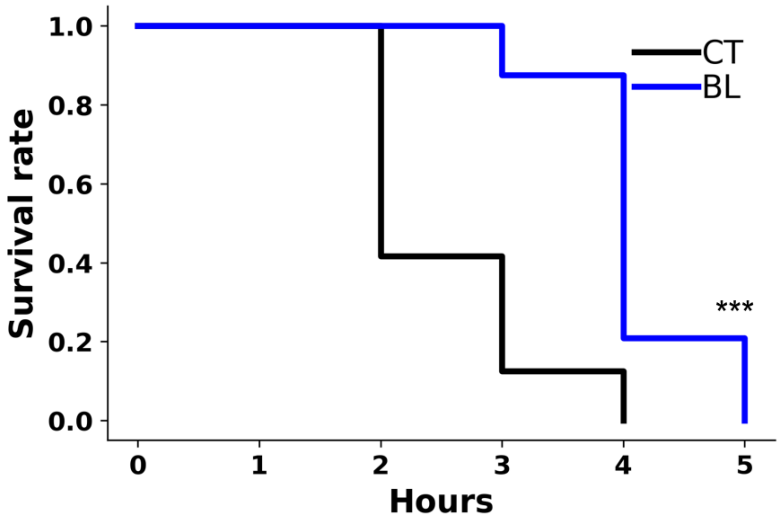

Fig. 6 BL increased the oxidative stress tolerance to hydrogen peroxide.

Synchronized N2 nematodes were grown on OP or BL plates for 96 hours and then transferred to 0.3% hydrogen peroxide (hour 0) and the survival rate of N2 nematodes was measured in every hour. 400 μl hydrogen peroxide was added to 24-well plates. N=24. Data were presented as the *Kaplan-Meier* curve, and ***P < 0.05 according to the conducted *log-rank test*.

Fig. 7 Oxidative stress tolerance (paraquat)

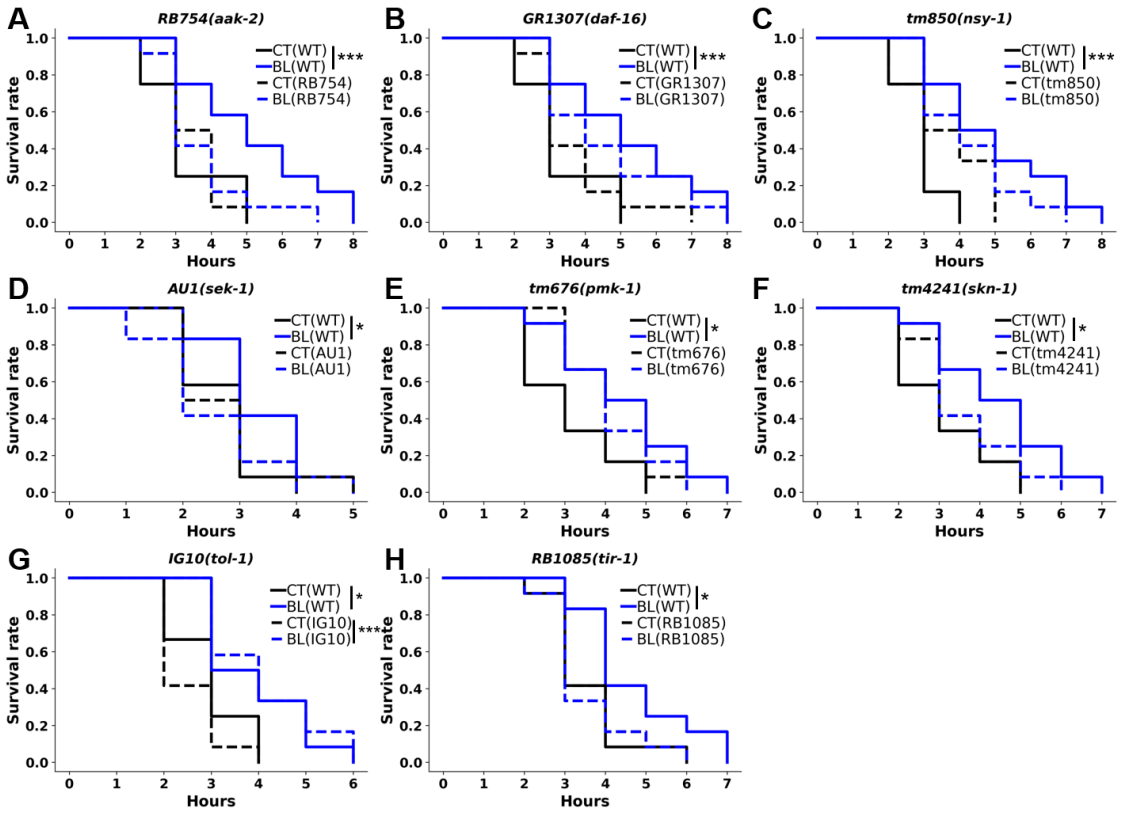

Fig. 7 BL increased the oxidative stress tolerance to paraquat.

Synchronized worms were grown on OP or BL plates for 96 hours and then transferred to 300 mM paraquat (hour 0) and the survival rate of N2 nematodes was measured in every hour. 400 µl paraquat was added to 24-well plates. Survival rate of nematodes and (A) RB754, (B) GR1307, (C) tm850, (D) AU1, (E) tm676, (F) tm4241, (G) IG10 and (H)

RB1085 in paraquat solution. N=12. Data were presented as the *Kaplan-Meier* curve, and *P < 0.05, ***P < 0.005 according to the conducted *log-rank test*.

Fig. 8 Oxidative stress tolerance (paraquat)

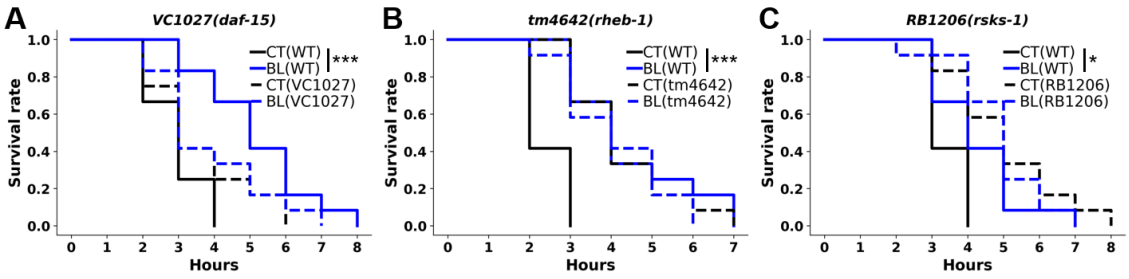

Fig. 8 BL increased the oxidative stress tolerance to paraquat.

Survival rate of N2 wild-type nematodes and (A) VC1027, (B) tm4642 and (C) RB1206 in 300 mM paraquat solution. N=12. Data were presented as the *Kaplan-Meier* curve, and *P < 0.05, ***P < 0.005 according to the conducted *log-rank test*.

Fig. 9 DAF-16 nuclei localization

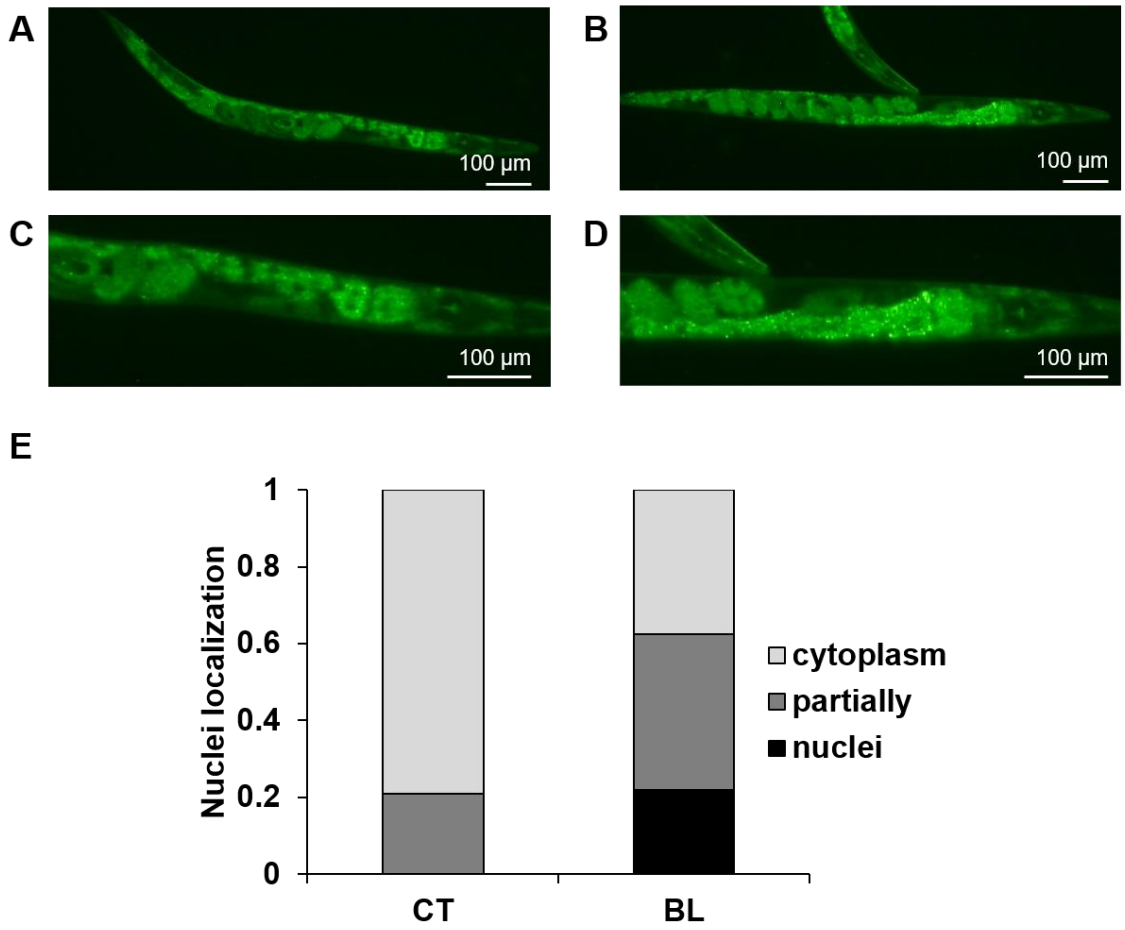

Fig. 9 BL induced nuclei localization of DAF-16.

Synchronized TJ356(*daf-16*::GFP) nematodes were grown on OP or BL plates for 96 hours. After washing the nematodes with S-basal, they are fixed with 10% ethanol for 10 min. The picture of (A) CT and (B) BL worm taken with BZ8000. (C) and (D) are the

high magnification images of (A) and (B) respectively. Scale bars indicate 100 μm. (E) Analyzed data from pictures. The subcellular localization of fluorescence was classified into three groups: mainly localized to the nucleus (nuclei), partially localized to the nucleus (partial), and localized to the cytoplasm (cytoplasm), and the proportions were shown [82]. Nuclei localization is indicated by bright small spots. N≥20.

Fig. 10 Intercellular ROS

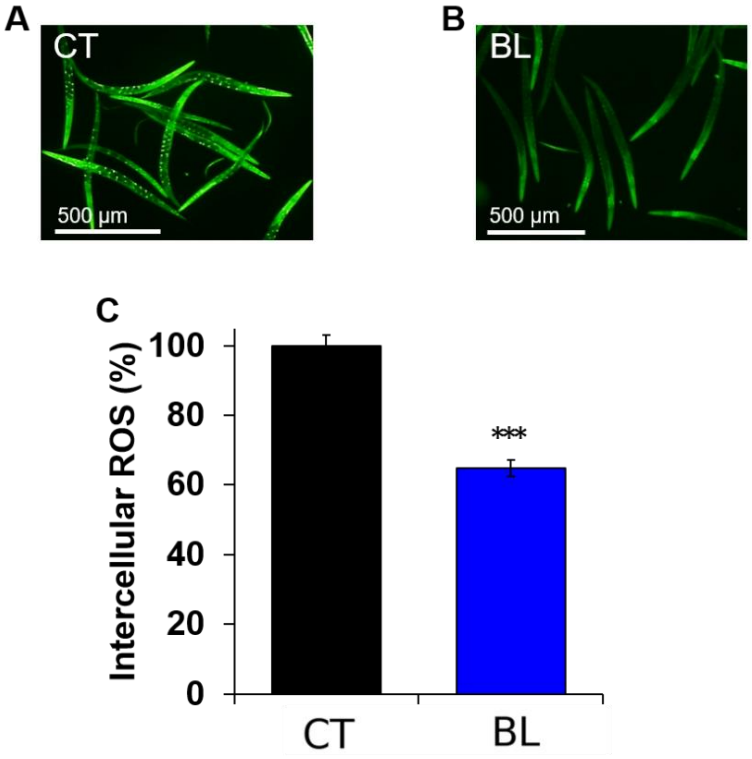

Fig. 10 BL reduced intercellular ROS.

Synchronized N2 nematodes were grown on OP or BL plates for 96 hours. After washing the nematodes with S-basal, 400 μl of DCF-DA solution was added and stirred for 1 hour. Then, after fixation with 10% ethanol for 10 min, the amount of intracellular ROS was measured by fluorescence microscope. ROS was stained with 50 μM DCF-DA. The picture of (A) CT and (B) BL worms taken with BZ8000. Scale bars indicate 500 μm. (C)

Analyzed data from pictures with ImageJ. N≥39. Data were presented as the mean ± SEM, and ***P < 0.005 according to the conducted *Student's t-test*.

Fig. 11 Gene expression

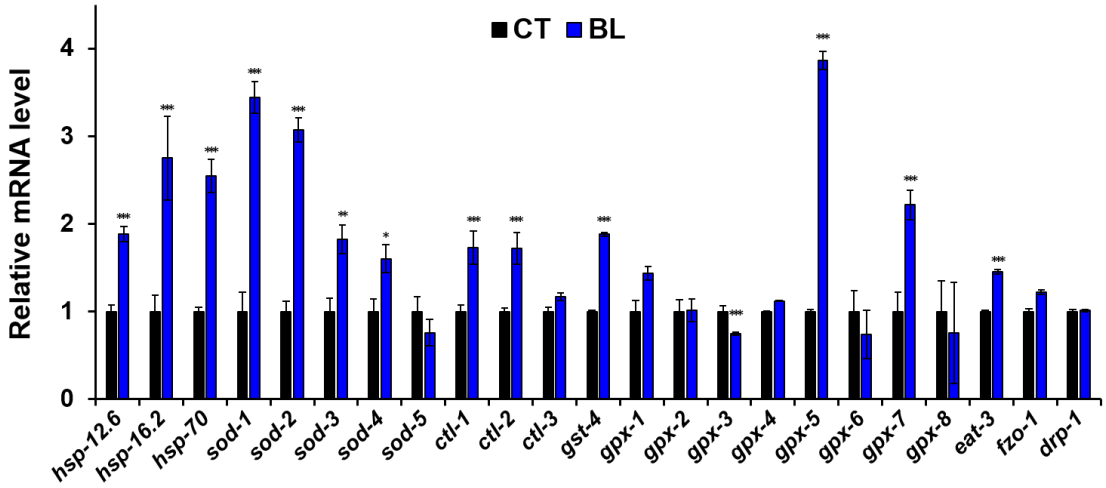

Fig. 11 BL upregulated the expression of mRNA related to stress tolerance and mitochondrial homeostasis.

mRNA level of adult N2 wild-type nematodes grown on OP plates or BL plates. FUdR was added on days -1, 0, and 3. mRNA of day 3 nematodes was extracted. Each sample mRNA was measured in three wells. Data were presented as the mean ± SEM, and * $P < 0.05$, ** $P < 0.01$, *** $P < 0.005$, according to the conducted *Student's t-test*.

Fig. 12 Life span

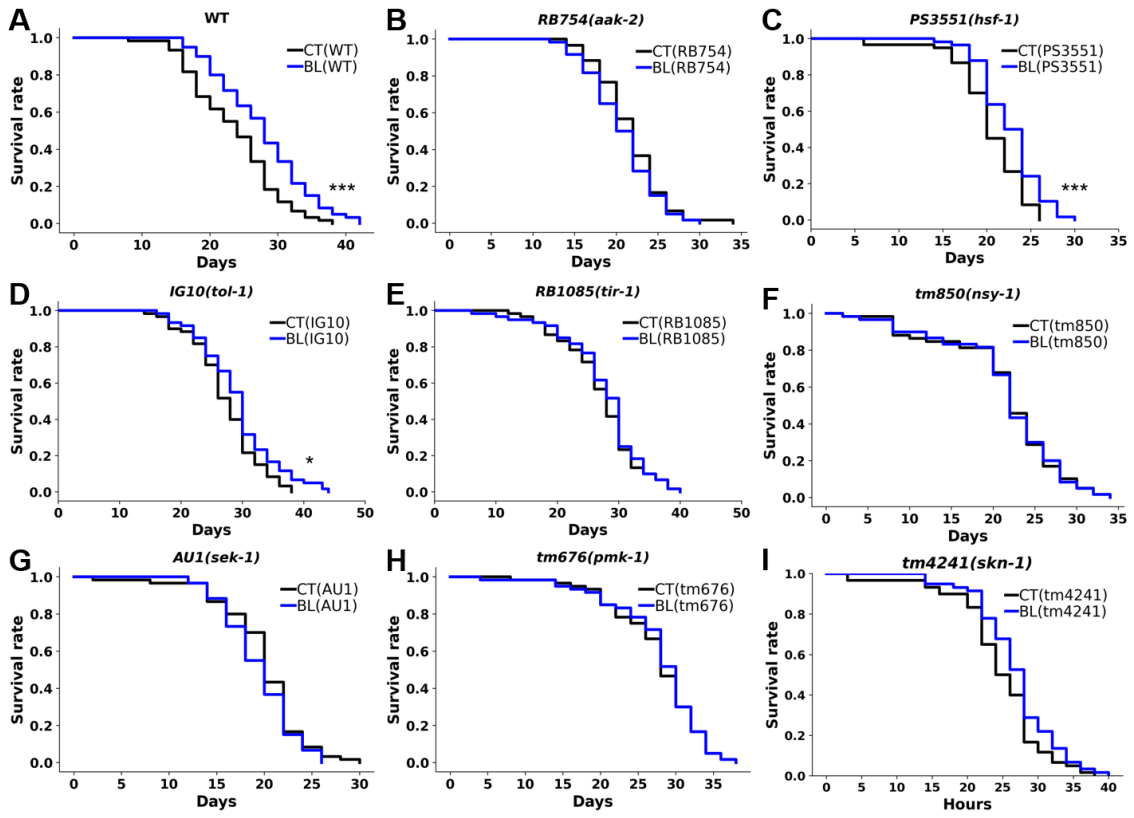

Fig. 12 BL extended the life span.

Synchronized nematodes were grown on OP plates for 96 hours and then transferred to OP or BL plates (day 0). Thereafter, the plates were changed every 2 days and the survival rate nematodes was measured. Survival was determined by nematode movements by gentle contact stimulation using a platinum picker. FUdR was added at day -1, 0, 2 and 4 to suppress egg laying and development. Survival rate of the adult nematodes of (A) N2

wild-type, (B) RB754, (C) PS3551, (D) IG10, (E) RB1085, (F) tm850, (G) AU1, (H) tm676 and (I) tm4241 grown on OP plates or BL plates every two days. N=60. Data were presented as the *Kaplan-Meier* curve, and *P < 0.05, ***P < 0.005 according to the conducted *log-rank test*.

Fig. 13 Egg laying

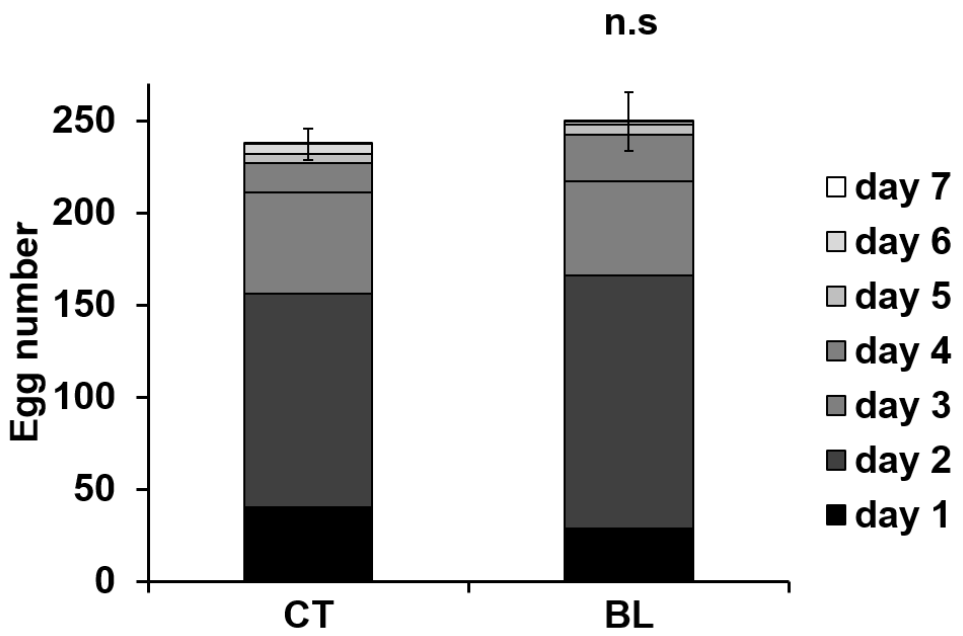

Fig. 13 BL did not change the egg laying.

Synchronized N2 nematodes were grown on OP or BL plates for 48 hours and then transferred to new OP or BL plates (day 0). Thereafter, the plates were changed every day and the number of eggs was measured. Each day indicates 48, 72, 96, 120, 144, 168 and 192 hours after synchronization. N=10. Data were presented as the mean ± SEM, no significance according to the conducted *Student's t-test*.

Fig. 14 Food intake

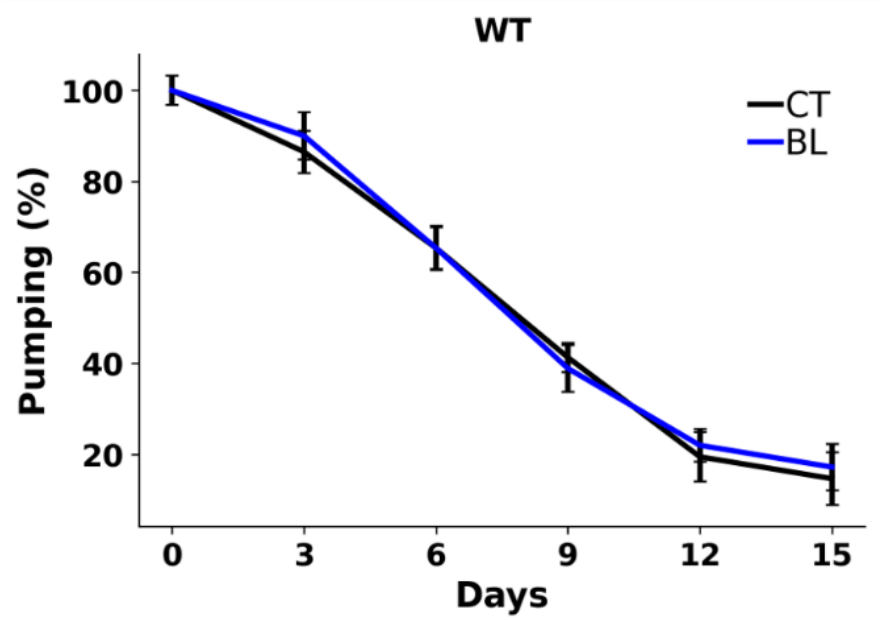

Fig. 14 BL did not change the food intake.

Synchronized N2 nematodes were grown on OP plates for 96 hours and then transferred to OP or BL plates (day 0). Thereafter, the plates were changed every 3 days and the number of pumping rate of N2 wild-type was measured for 15s. *C. elegans* intakes food simultaneously with pharyngeal movements. FUdR was added at day -1, 0 and 3. N=10. Data were presented as the mean ± SEM, no significance according to the conducted *Student's t-test*. The pumpings at day 0 are shown in the result as 100.

Fig. 15 Age-related motility

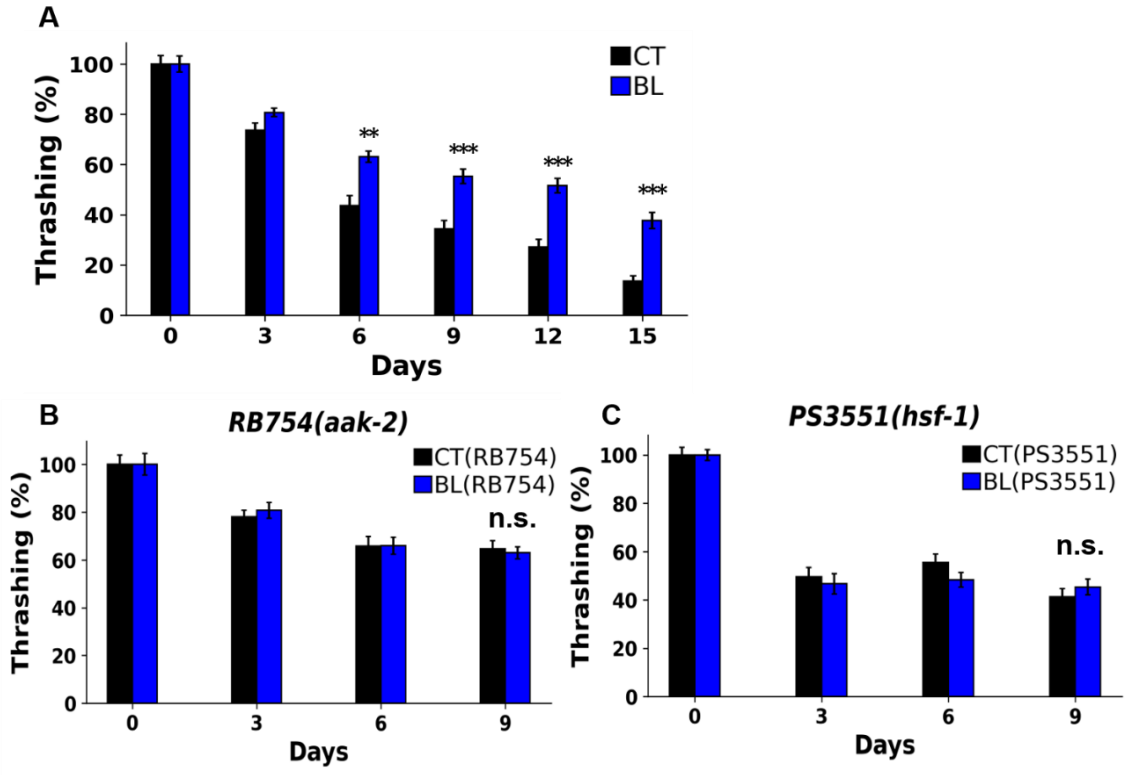

Fig. 15 BL inhibited the age-related retardation of motility.

Synchronized nematodes were grown on OP plates for 96 hours and then transferred to OP or BL plates (day 0). Thereafter, the plates were changed every 3 days and the number of thrashing movements of nematodes was measured for 15s. On the day -1, 0, and 3, 0.5 mg/ml FUdR was used to inhibit egg laying and development. Motility rate of the adult nematodes of (A) N2 wild-type, (B) RB754 and (C) PS3551 grown on OP plates or BL

plates every 3 days. N=10, Data were presented as the mean ± SEM, and ***P < 0.01, ***P < 0.005 (vs CT at the same time period) according to the conducted *Student's t-test*.

Fig. 16 Fat accumulation

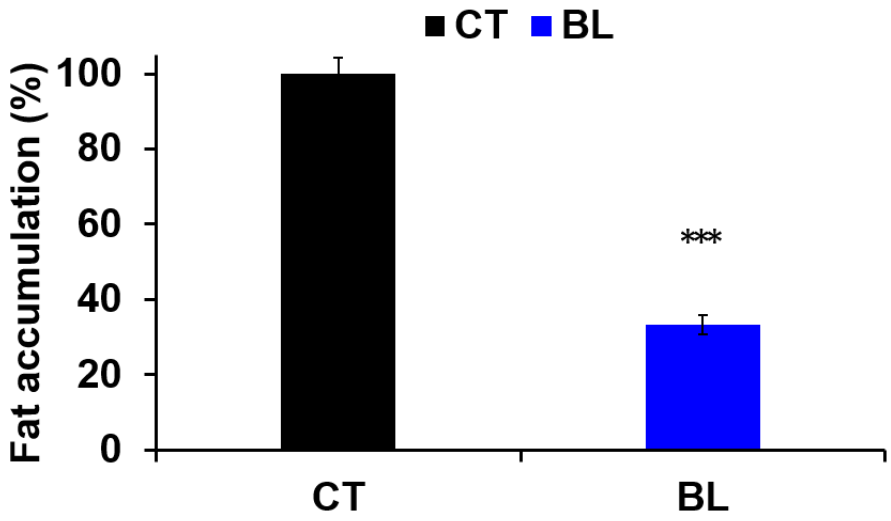

Fig. 16 BL decreased the fat accumulation.

Synchronized N2 wild-type nematodes were grown on OP or BL plates for 96 hours. Thereafter, they were fixed with 4% paraformaldehyde for 2 hours at 4°C. After washing with S-basal, 400 µl of 5 µg/ml Nile Red staining solution was added and the samples were stirred for 10 min at 4 °C. The mixtures were washed twice with S-basal again and measured by a fluorescence microscope BZ8000. N≥26. Data were presented as the mean ± SEM, ***P < 0.005 according to the conducted *Student's t-test*.

Fig. 17 Muscle mass

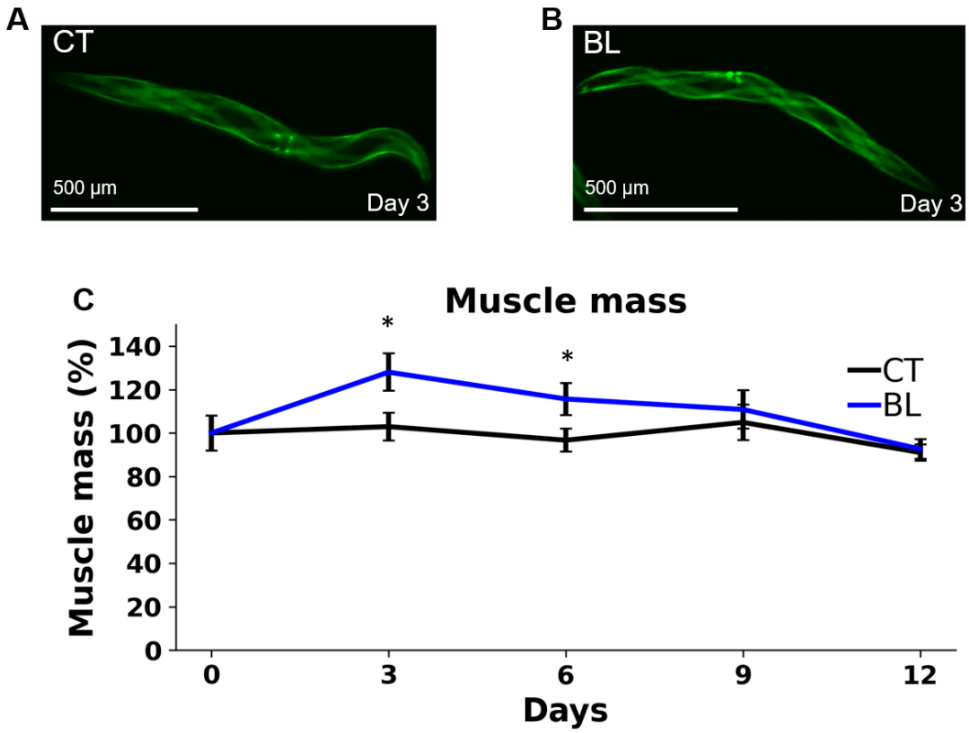

Fig. 17 BL increased muscle mass.

Synchronized nematodes RW1596(*myo-3*::GFP) were grown on OP plates for 96 hours and then transferred to OP or BL plates (day 0). Thereafter, the plates were changed every 3 days and GFP fluorescence was measured with a fluorescent microscope BZ-X810. On the day -1, 0, and 3, 0.5 mg/ml FUdR was used to inhibit egg laying and development. The picture of (A) CT and (B) BL worm at day 3 taken with BZ-X810. Scale bars indicate 500 µm. (C) Analyzed data from pictures with ImageJ. N≥13. Data were presented as the

mean ± SEM, and *P < 0.05 (vs CT at the same time period) according to the conducted *Student's t-test*.

Fig. 18 Mitochondrial mass, morphohlogy

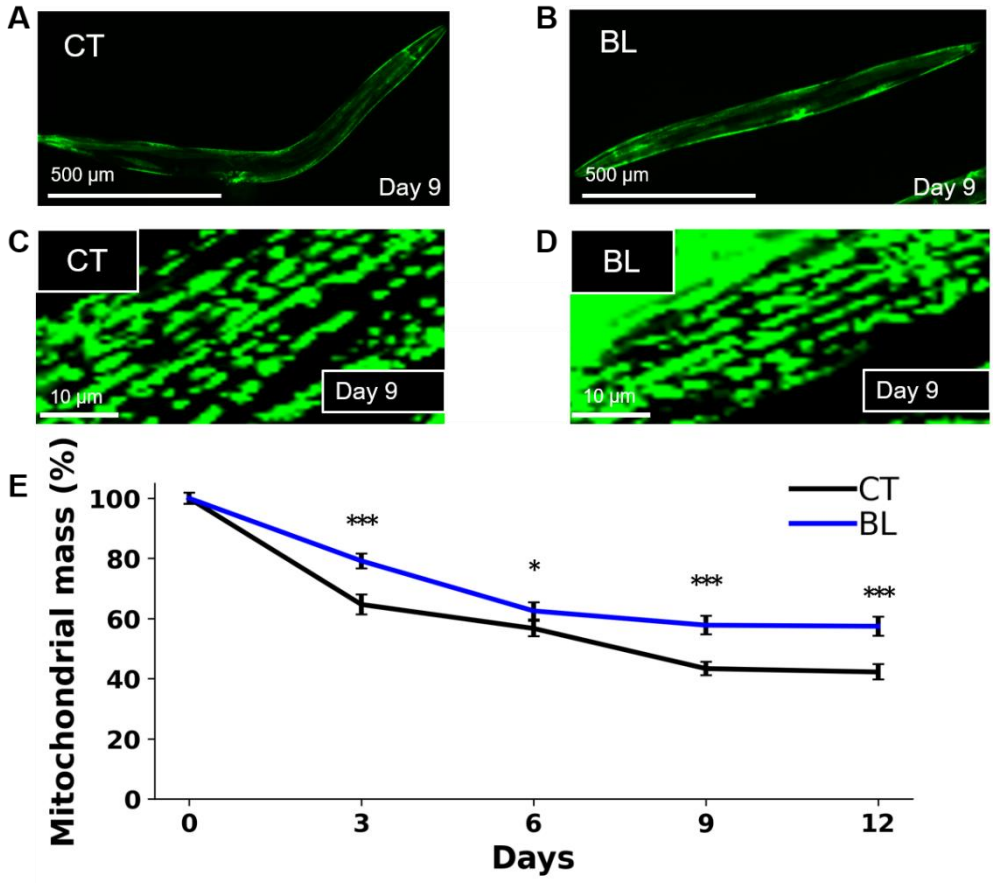

Fig. 18 BL inhibited the decrease in intramuscular mitochondrial content and maintained homeostasis.

Synchronized nematodes SJ4103(*myo-3*::GFP(mit)) were grown on OP plates for 96 hours and then transferred to OP or BL plates (day 0). Thereafter, the plates were changed every 3 days and GFP fluorescence was measured with a fluorescent microscope. On the day -1, 0, and 3, 0.5 mg/ml FUdR was used to inhibit egg laying and development. The

picture of (A) CT and (B) BL worm at day 9 taken with BZ-X810, and (C) CT and (D) BL taken with THUNDER imaging system. Scale bars indicate 500 μm in (A) and (B), and 10 μm in (C) and (D). (E) Analyzed data from pictures with ImageJ. N≥11. Data were presented as the mean ± SEM, and *P < 0.05, ***P < 0.005 (vs CT at the same time period) according to the conducted *Student's t-test*.

Fig. 19 ATP

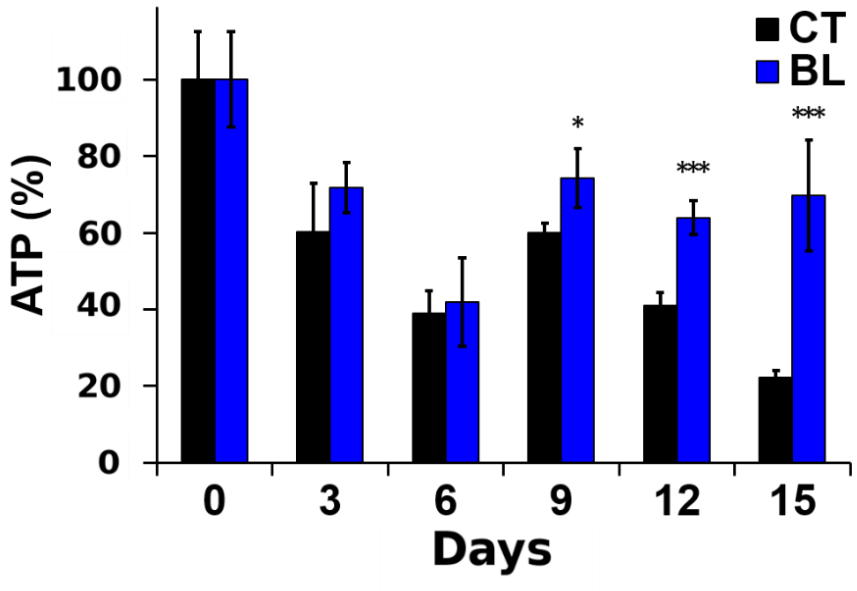

Fig. 19 BL prevented the decline of ATP.

Synchronized N2 nematodes were grown on OP plates for 96 hours and then transferred to OP or BL plates (day 0). On the day -1, 0, and 3, as well as motility measurements, 0.5 mg/ml FUdR was used to inhibit spawning and development. More than 200 nematodes were collected and washed with MilliQ, and then crashed with Bio Masher II and Power Masher II every 3 days. The crushed fluid was cooled and centrifuged (4°C, 1,000 g, 10 min.) and ATP was extracted using the "Tissue" ATP assay kit. Luciferase luminescence was then quantified using a white 96-well plate and a luminometer. Each sample ATP

was measured in three wells. Data were presented as the mean ± SEM, and *P < 0.05, ***P < 0.005 (vs CT at the same time period) according to the conducted *Student's t-test*.

Fig. 20 Mitochondrial membrane potential

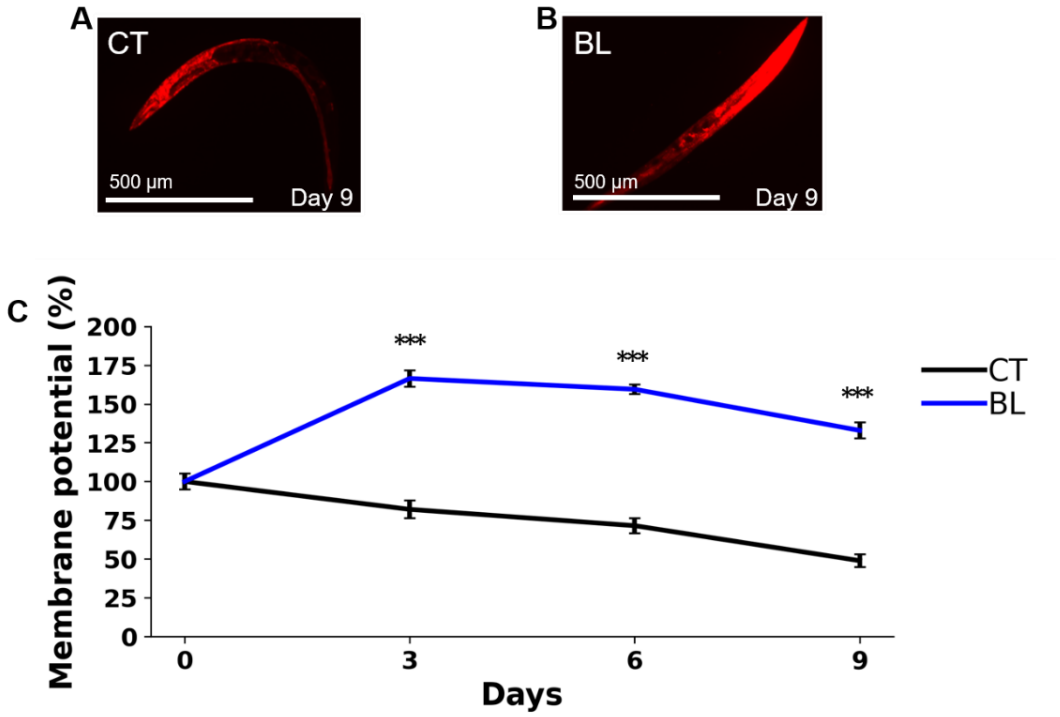

Fig. 20 BL suppressed the decrease in mitochondrial membrane potential.

Synchronized nematodes SJ4103(*myo-3*::GFP(mit)) nematodes were grown on OP plates for 96 hours and then transferred to OP or BL plates (day 0). Thereafter, the plates were changed every 3 days. 1 ml of 0.5 μM MitoTracker Orange CMTMRos was added. 3 hours later, the samples were collected and washed. Thereafter, nematodes were fixed in 10% ethanol for 10 mins and the fluorescence of MitoTracker was measured. On the day -1, 0, and 3, as well as motility measurements, 0.5 mg/ml FUdR was used to inhibit spawning and development. The picture of (A) CT and (B) BL worm at day 9 taken with

BZ-X810. Scale bars indicate 500 µm. (C) Analyzed data from pictures with ImageJ. N≥13. Data were presented as the mean ± SEM, and ***P < 0.005 (vs CT at the same time period) according to the conducted *Student's t-test*.

Fig. 21 Mitochondrial ROS

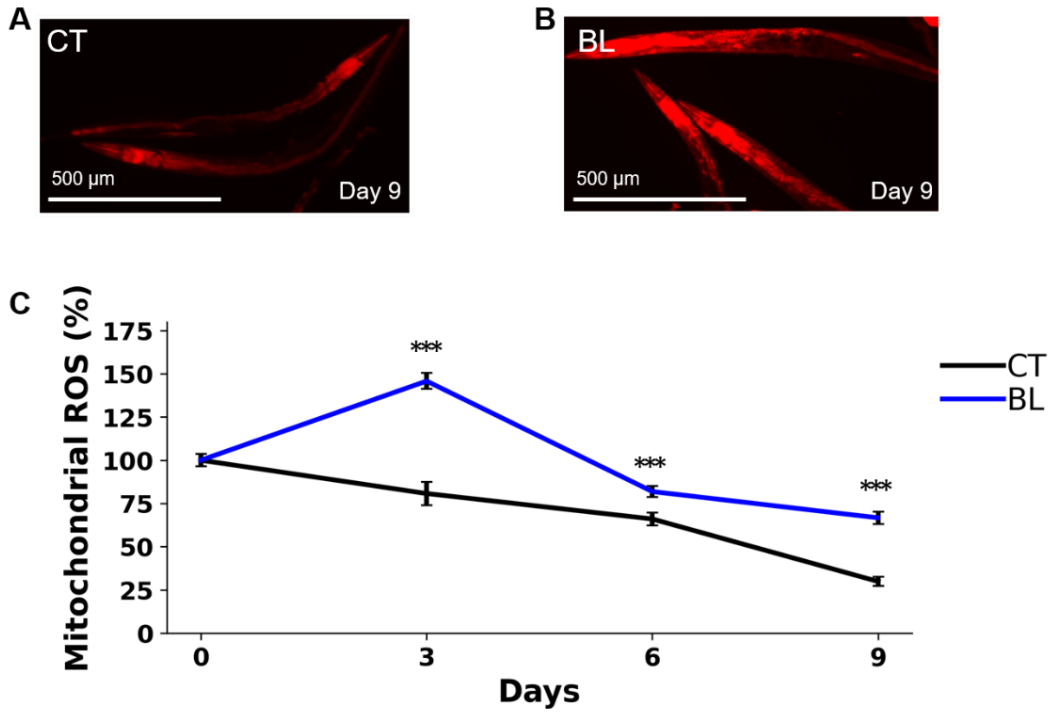

Fig. 21 BL suppressed the decrease in mitochondrial ROS over time.

Synchronized nematodes SJ4103(*myo-3*::GFP(mit)) nematodes were grown on OP plates for 96 hours and then transferred to OP or BL plates (day 0). Thereafter, the plates were changed every 3 days. 1 ml of 0.5 µM MitoTracker Orange CM-H2TMRos was added. 3 hours later, the samples were collected and washed. Thereafter, nematodes were fixed in 10% ethanol for 10 mins and the fluorescence of MitoTracker was measured. On the day -1, 0, and 3, as well as motility measurements, 0.5 mg/ml FUdR was used to inhibit spawning and development. The picture of (A) CT and (B) BL worm at day 9 taken with

BZ-X810. Scale bars indicate 500 µm. (C) Analyzed data from pictures with ImageJ. N≥11. Data were presented as the mean ± SEM, and ***P < 0.005 (vs CT at the same time period) according to the conducted *Student's t-test*.

Fig. 22 Age-relted motility with mitochondrial inhibitors

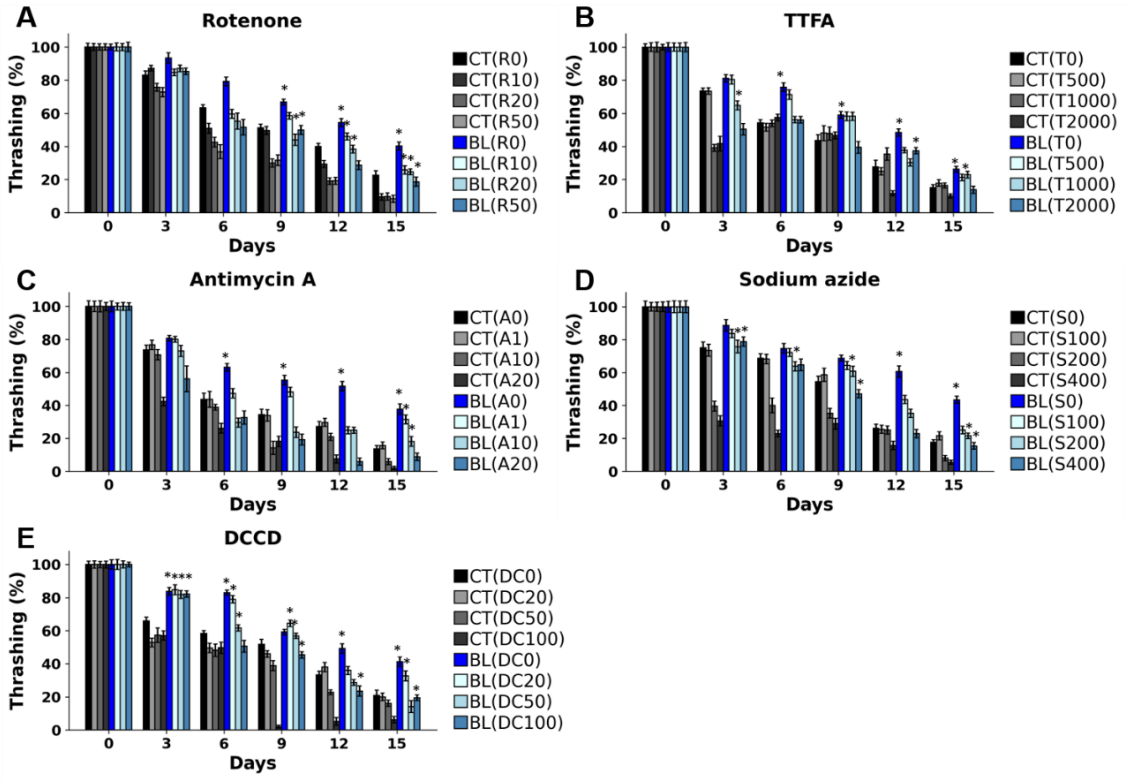

Fig. 22 All mitochondrial complex inhibitor were involved in the upregulation of age-related motility by BL.

Motility rate of the adult N2 wild-type nematodes, adding (A) rotenone, (B) TTFA, (C) antimycin A, (D) sodium azide and (E) DCCD grown on OP plates or BL plates every 3 days. FUdR was added at day -1, 0, and 3. N=10. Data were presented as the mean ± SEM,

and *P < 0.05 (vs CT at the same time period) according to the conducted one way ANOVA followed by *Tukey's HSD* post hoc test

Fig. 23 Mitochondrial membrane potential with mitochondrial inhibitors

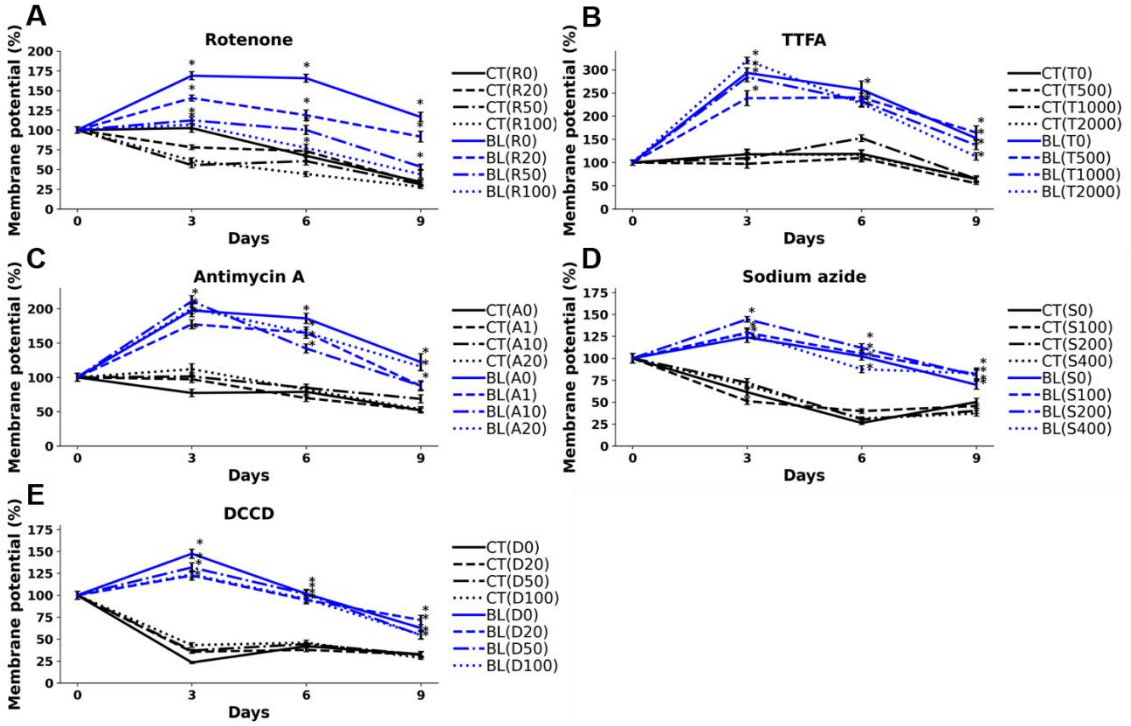

Fig. 23 Part of mitochondrial complex inhibitor was involved in the upregulation of mitochondrial membrane potential by BL.

Mitochondrial membrane potential level of the adult SJ4103(*myo-3*::GFP(mit)) nematodes, adding (A) rotenone, (B) TTFA, (C) antimycin A, (D) sodium azide and (E) DCCD grown on OP plates or BL plates every 3 days. FUdR was added at day -1, 0, and 3. N≥13 for vehicle, ≥13 for rotenone, ≥13 for TTFA, ≥11 for antimycin A, ≥10 for sodium azide, ≥10 for DCCD. Data were presented as the mean ± SEM, and *P < 0.005

(vs CT at the same concentration of inhibitors) according to the conducted one way ANOVA followed by *Tukey's HSD* post hoc test.

Acknowledgements

I would like to express my respect to associate professor Sakamoto for his guidance in this research and really appreciate the offer of BR-108 to Combi Corporation.

References

1. Nations U, United Nations. World Population Prospects, The 2019 Revision - Volume I: Comprehensive Tables. 2019. doi:10.18356/15994a82-en

2. Kaeberlein M. How healthy is the healthspan concept? Geroscience. 2018;40: 361–364.

3. Japanese Cabinet Office. Annual Report on the Ageing Society FY 2019.pdf. 2019. Available: https://www8.cao.go.jp/kourei/whitepaper/index-w.html

4. Siemann EH, Creasy LL. Concentration of the Phytoalexin Resveratrol in Wine. Am J Enol Vitic. 1992;43: 49–52.

5. Renaud S, de Lorgeril M. Wine, alcohol, platelets, and the French paradox for coronary heart disease. Lancet. 1992;339: 1523–1526.

6. Li H, Xia N, Hasselwander S, Daiber A. Resveratrol and Vascular Function. Int J Mol Sci. 2019;20. doi:10.3390/ijms20092155

7. Gülçin İ. Antioxidant properties of resveratrol: A structure–activity insight. Innov Food Sci Emerg Technol. 2010;11: 210–218.

8. Hung LM, Chen JK, Huang SS, Lee RS, Su MJ. Cardioprotective effect of resveratrol, a natural antioxidant derived from grapes. Cardiovasc Res. 2000;47: 549–555.

9. Carrizzo A, Forte M, Damato A, Trimarco V, Salzano F, Bartolo M, et al. Antioxidant effects of resveratrol in cardiovascular, cerebral and metabolic diseases. Food Chem Toxicol. 2013;61: 215–226.

10. Morselli E, Maiuri MC, Markaki M, Megalou E, Pasparaki A, Palikaras K, et al. Caloric restriction and resveratrol promote longevity through the Sirtuin-1-dependent induction of autophagy. Cell Death Dis. 2010;1: e10.

11. Timmers S, Auwerx J, Schrauwen P. The journey of resveratrol from yeast to human. Aging . 2012;4: 146.

12. Wood JG, Rogina B, Lavu S, Howitz K, Helfand SL, Tatar M, et al. Sirtuin activators mimic caloric restriction and delay ageing in metazoans. Nature. 2004;430: 686–689.

13. Imai S, Armstrong CM, Kaeberlein M, Guarente L. Transcriptional silencing and longevity protein Sir2 is an NAD-dependent histone deacetylase. Nature. 2000;403: 795–800.

14. Li W, Zhang B, Tang J, Cao Q, Wu Y, Wu C. Sirtuin 2, a mammalian homolog of yeast silent information regulator-2 longevity regulator, is an oligodendroglial protein that decelerates cell differentiation through …. Journal of. 2007. Available: https://www.jneurosci.org/content/27/10/2606.short

15. Singh S, Kumar PU, Thakur S, Kiran S, Sen B, Sharma S, et al. Expression/localization patterns of sirtuins (SIRT1, SIRT2, and SIRT7) during progression of cervical cancer and effects of sirtuin inhibitors on growth of cervical cancer cells. Tumor Biology. 2015;36: 6159–6171.

16. Tissenbaum HA, Ruvkun G. An insulin-like signaling pathway affects both longevity and reproduction in *Caenorhabditis elegans*. Genetics. 1998;148: 703–717.

17. Lin K, Hsin H, Libina N, Kenyon C. Regulation of the *Caenorhabditis elegans* longevity protein DAF-16 by insulin/IGF-1 and germline signaling. Nat Genet. 2001;28: 139–145.

18. Hesp K, Smant G, Kammenga JE. *Caenorhabditis elegans* DAF-16/FOXO transcription factor and its mammalian homologs associate with age-related disease. Exp Gerontol. 2015;72: 1–7.

19. Lapierre LR, Hansen M. Lessons from *C. elegans*: signaling pathways for longevity. Trends Endocrinol Metab. 2012;23: 637–644.

20. Kaspar JW, Niture SK, Jaiswal AK. Nrf2:INrf2 (Keap1) signaling in oxidative stress. Free Radic Biol Med. 2009;47: 1304–1309.

21. Troemel ER, Chu SW, Reinke V, Lee SS, Ausubel FM, Kim DH. p38 MAPK regulates expression of immune response genes and contributes to longevity in *C. elegans*. PLoS Genet. 2006;2: e183.

22. Oh SW, Mukhopadhyay A, Svrzikapa N, Jiang F, Davis RJ, Tissenbaum HA. JNK regulates lifespan in *Caenorhabditis elegans* by modulating nuclear translocation of forkhead transcription factor/DAF-16. Proc Natl Acad Sci U S A. 2005;102: 4494–4499.

23. Morley JF, Morimoto RI. Regulation of longevity in *Caenorhabditis elegans* by heat shock factor and molecular chaperones. Mol Biol Cell. 2004;15: 657–664.

24. Blackwell TK, Sewell AK, Wu Z, Han M. TOR Signaling in *Caenorhabditis elegans* Development, Metabolism, and Aging. Genetics. 2019;213: 329–360.

25. Zheng S, Chiu H, Boudreau J, Papanicolaou T, Bendena W, Chin-Sang I. A functional study of all 40 *Caenorhabditis elegans* insulin-like peptides. J Biol Chem. 2018;293: 16912–16922.

26. Wang Y, Tissenbaum HA. Overlapping and distinct functions for a *Caenorhabditis elegans* SIR2 and DAF-16/FOXO. Mech Ageing Dev. 2006;127: 48–56.

27. Huang H, Tindall DJ. Dynamic FoxO transcription factors. J Cell Sci. 2007;120: 2479–2487.

28. Galbadage T, Shepherd TF, Cirillo SLG, Gumienny TL, Cirillo JD. The *Caenorhabditis elegans* p38 MAPK Gene plays a key role in protection from mycobacteria. Microbiologyopen. 2016;5: 436–452.

29. Tenor JL, Aballay A. A conserved Toll-like receptor is required for *Caenorhabditis elegans* innate immunity. EMBO Rep. 2008;9: 103–109.

30. Cheesman HK, Feinbaum RL, Thekkiniath J, Dowen RH, Conery AL, Pukkila-Worley R. Aberrant Activation of p38 MAP Kinase-Dependent Innate Immune Responses Is Toxic to *Caenorhabditis elegans*. G3 . 2016;6: 541–549.

31. Inoue H, Hisamoto N, An JH, Oliveira RP, Nishida E, Blackwell TK, et al. The *C. elegans* p38 MAPK pathway regulates nuclear localization of the transcription factor SKN-1 in oxidative stress response. Genes Dev. 2005;19: 2278–2283.

32. Mukhopadhyay A, Oh SW, Tissenbaum HA. Worming pathways to and from DAF-16/FOXO. Exp Gerontol. 2006;41: 928–934.

33. Hsu A-L, Murphy CT, Kenyon C. Regulation of aging and age-related disease by DAF-16 and heat-shock factor. Science. 2003;300: 1142–1145.

34. Jia K, Chen D, Riddle DL. The TOR pathway interacts with the insulin signaling pathway to regulate *C. elegans* larval development, metabolism and life span. Development. 2004;131: 3897–3906.

35. Bernet MF, Brassart D, Neeser JR, Servin AL. Adhesion of human bifidobacterial strains to cultured human intestinal epithelial cells and inhibition of enteropathogen-cell interactions. Appl Environ Microbiol. 1993;59: 4121–4128.

36. Mitsuoka T. Taxonomy and Ecology of Bifidobacteria. Bifidobact Microflora. 1984;3: 11–28.

37. Sekirov I, Russell SL, Antunes LCM, Finlay BB. Gut microbiota in health and disease. Physiol Rev. 2010;90: 859–904.

38. Reuter G. The Lactobacillus and Bifidobacterium microflora of the human intestine: composition and succession. Curr Issues Intest Microbiol. 2001;2: 43–53.

39. Requena T, Burton J, Matsuki T, Munro K, Simon MA, Tanaka R, et al. Identification, detection, and enumeration of human bifidobacterium species by PCR targeting the transaldolase gene. Appl Environ Microbiol. 2002;68: 2420–2427.

40. Picard C, Fioramonti J, Francois A, Robinson T, Neant F, Matuchansky C. bifidobacteria as probiotic agents--physiological effects and clinical benefits. Aliment Pharmacol Ther. 2005;22: 495–512.

41. Hütt P, Shchepetova J, Loivukene K, Kullisaar T, Mikelsaar M. Antagonistic activity of probiotic lactobacilli and bifidobacteria against entero-and uropathogens. J Appl Microbiol. 2006;100: 1324–1332.

42. Chick H, Shin HS, Ustunol Z. Growth and Acid Production by Lactic Acid Bacteria and Bifidobacteria Grown in Skim Milk Containing Honey. J Food Sci. 2001;66: 478–481.

43. MITSUOKA, T. Die Darmflora bei Menschen. I. Mitteilung. Die Zusammensetzung der Faekalflora der verschiedenen Altersgruppen. Zbl Bakt Hyg I Abt Orig A. 1972;233: 333–342.

44. Mitsuoka T. Bifidobacteria and their role in human health. J Ind Microbiol. 1990;6: 263–267.

45. Anukam KC, Reid G. Probiotics: 100 years (1907--2007) after Elie Metchnikoff's observation. Communicating current research and educational topics and trends in applied microbiology. 2007;1: 466–474.

46. Ruiz L, Delgado S, Ruas-Madiedo P, Sánchez B, Margolles A. Bifidobacteria and Their Molecular Communication with the Immune System. Front Microbiol. 2017;8: 2345.

47. Grönlund M-M, Gueimonde M, Laitinen K, Kociubinski G, Grönroos T, Salminen S, et al. Maternal breast-milk and intestinal bifidobacteria guide the compositional development of the Bifidobacterium microbiota in infants at risk of allergic disease. Clinical & Experimental Allergy. 2007;37: 1764–1772.

48. Singh J, Rivenson A, Tomita M, Shimamura S, Ishibashi N, Reddy BS. *Bifidobacterium longum*, a lactic acid-producing intestinal bacterium inhibits colon cancer and modulates the intermediate biomarkers of colon carcinogenesis. Carcinogenesis. 1997;18: 833–841.

49. Foster JA, McVey Neufeld K-A. Gut–brain axis: how the microbiome influences anxiety and depression. Trends Neurosci. 2013;36: 305–312.

50. Ticinesi A, Lauretani F, Milani C, Nouvenne A, Tana C, Del Rio D, et al. Aging Gut Microbiota at the Cross-Road between Nutrition, Physical Frailty, and Sarcopenia: Is There a Gut–Muscle Axis? Nutrients. 2017;9: 1303.

51. Grosicki GJ, Fielding RA, Lustgarten MS. Gut Microbiota Contribute to Age-Related Changes in Skeletal Muscle Size, Composition, and Function: Biological Basis for a Gut-Muscle Axis. Calcif Tissue Int. 2018;102: 433–442.

52. Arboleya S, Watkins C, Stanton C, Ross RP. Gut Bifidobacteria Populations in Human Health and Aging. Front Microbiol. 2016;7: 1204.

53. Knight CG, Patel MN, Azevedo RBR, Leroi AM. A novel mode of ecdysozoan growth in *Caenorhabditis elegans*. Evol Dev. 2002;4: 16–27.

54. Stiernagle T. Maintenance of *C. elegans*. WormBook. 2006; 1–11.

55. Nigon VM, Félix M-A. History of research on *C. elegans* and other free-living nematodes as model organisms. WormBook. 2017;2017: 1–84.

56. Son HG, Altintas O, Kim EJE, Kwon S, Lee S-JV. Age-dependent changes and biomarkers of aging in *Caenorhabditis elegans*. Aging Cell. 2019;18: e12853.

57. Kim W, Underwood RS, Greenwald I, Shaye DD. OrthoList 2: A New Comparative Genomic Analysis of Human and *Caenorhabditis elegans* Genes. Genetics. 2018;210: 445–461.

58. Brenner S. The genetics of *Caenorhabditis elegans*. Genetics. 1974;77: 71–94.

59. Alexander AG, Marfil V, Li C. Use of *Caenorhabditis elegans* as a model to study Alzheimer's disease and other neurodegenerative diseases. Front Genet. 2014;5: 279.

60. Cooper JF, Van Raamsdonk JM. Modeling Parkinson's Disease in *C. elegans*. J Parkinsons Dis. 2018;8: 17–32.

61. Fire A, Xu S, Montgomery MK, Kostas SA, Driver SE, Mello CC. Potent and specific genetic interference by double-stranded RNA in *Caenorhabditis elegans*. Nature. 1998;391: 806–811.

62. Friedland AE, Tzur YB, Esvelt KM, Colaiácovo MP, Church GM, Calarco JA. Heritable genome editing in *C. elegans* via a CRISPR-Cas9 system. Nat Methods. 2013;10: 741–743.

63. Dirksen P, Marsh SA, Braker I, Heitland N, Wagner S, Nakad R, et al. The native microbiome of the nematode *Caenorhabditis elegans*: gateway to a new host-microbiome model. BMC Biol. 2016;14: 38.

64. Zhang F, Berg M, Dierking K, Félix M-A, Shapira M, Samuel BS, et al. *Caenorhabditis elegans* as a Model for Microbiome Research. Front Microbiol. 2017;8: 485.

65. Thammawong N, Takahashi H, Sugawara T, Sakamoto K, Others. α-Mangostin Promotes DAF-16-Mediated Thermotolerance in *Caenorhabditis elegans*. Food Nutr Sci. 2018;9: 693.

66. Sugawara T, Sakamoto K. Killed *Bifidobacterium longum* enhanced stress tolerance and prolonged life span of *Caenorhabditis elegans* via DAF-16. Br J Nutr. 2018;120: 872–880.

67. Sugawara T, Saraprug D, Sakamoto K. Soy sauce increased the oxidative stress tolerance of nematode via p38 MAPK pathway. Biosci Biotechnol Biochem. 2019;83: 709–716.

68. Sugawara T, Furuhashi T, Shibata K, Abe M, Kikuchi K, Arai M, et al. Fermented product of rice with Lactobacillus kefiranofaciens induces anti-aging effects and heat stress tolerance in nematodes via DAF-16. Biosci Biotechnol Biochem. 2019;83: 1484–1489.

69. Sugawara T, Sakamoto K. Quercetin enhances motility in aged and heat-stressed *Caenorhabditis elegans* nematodes by modulating both HSF-1 activity, and insulin-like and p38-MAPK signalling. PLoS One. 2020;15: e0238528.

70. Andersen ML, Winter LMF. Animal models in biological and biomedical research - experimental and ethical concerns. An Acad Bras Cienc. 2019;91: e20170238.

71. Avila D, Helmcke K, Aschner M. The *Caenorhabiditis elegans* model as a reliable tool in neurotoxicology. Hum Exp Toxicol. 2012;31: 236–243.

72. Komura T, Yasui C, Miyamoto H, Nishikawa Y. *Caenorhabditis elegans* as an alternative model host for legionella pneumophila, and protective effects of *Bifidobacterium infantis*. Appl Environ Microbiol. 2010;76: 4105–4108.

73. Komura T, Ikeda T, Yasui C, Saeki S, Nishikawa Y. Mechanism underlying prolongevity induced by bifidobacteria in *Caenorhabditis elegans*. Biogerontology. 2013;14: 73–87.

74. Martorell P, Llopis S, González N, Chenoll E, López-Carreras N, Aleixandre A, et al. Probiotic Strain *Bifidobacterium animalis* subsp. lactis CECT 8145 Reduces Fat Content and Modulates Lipid Metabolism and Antioxidant Response in *Caenorhabditis elegans*. J Agric Food Chem. 2016;64: 3462–3472.

75. Zhao L, Zhao Y, Liu R, Zheng X, Zhang M, Guo H, et al. The Transcription Factor DAF-16 is Essential for Increased Longevity in *C. elegans* Exposed to *Bifidobacterium longum* BB68. Sci Rep. 2017;7: 7408.

76. Sun S, Ohta A, Kuhara A, Nishikawa Y, Kage-Nakadai E. daf-16/FOXO isoform b in AIY neurons is involved in low preference for *Bifidobacterium infantis* in *Caenorhabditis elegans*. Neurosci Res. 2020;150: 8–16.

77. Sun S, Mizuno Y, Komura T, Nishikawa Y, Kage-Nakadai E. Toll-like receptor homolog TOL-1 regulates *Bifidobacterium infantis*-elicited longevity and behavior in *Caenorhabditis elegans*. Biosci Microbiota Food Health. 2019;38: 105–110.

78. Roselli M, Schifano E, Guantario B, Zinno P, Uccelletti D, Devirgiliis C. *Caenorhabditis elegans* and Probiotics Interactions from a Prolongevity Perspective. Int J Mol Sci. 2019;20. doi:10.3390/ijms20205020

79. Lee J, Choe J, Kim J, Oh S, Park S, Kim S, et al. Heat-killed Lactobacillus spp. cells enhance survivals of *Caenorhabditis elegans* against Salmonella and Yersinia infections. Lett Appl Microbiol. 2015;61: 523–530.

80. Nematode Growth Medium (NGM). Cold Spring Harb Protoc. 2014;2014: db.rec081299.

81. Zhang Y, Chen D, Smith MA, Zhang B, Pan X. Selection of Reliable Reference Genes in *Caenorhabditis elegans* for Analysis of Nanotoxicity. PLoS One. 2012;7: e31849.

82. Wang E, Wink M. Chlorophyll enhances oxidative stress tolerance in *Caenorhabditis elegans* and extends its lifespan. PeerJ. 2016;4: e1879.

83. James J, Fiji N, Roy D, Mg DA, Shihabudeen MS, Chattopadhyay D, et al. A rapid method to assess reactive oxygen species in yeast using H 2 DCF-DA. Anal Methods. 2015;7: 8572–8575.

84. Gandhi S, Santelli J, Mitchell DH, Stiles JW, Sanadi DR. A simple method for maintaining large, aging populations of *Caenorhabditis elegans*. Mech Ageing Dev. 1980;12: 137–150.

85. Avery L, Shtonda BB. Food transport in the *C. elegans* pharynx. J Exp Biol. 2003. Available: https://jeb.biologists.org/content/206/14/2441.short

86. Squier TC. Oxidative stress and protein aggregation during biological aging. Exp Gerontol. 2001;36: 1539–1550.

87. Murakami S, Johnson TE. A genetic pathway conferring life extension and resistance to UV stress in *Caenorhabditis elegans*. Genetics. 1996;143: 1207–1218.

88. Muñoz MJ. Longevity and heat stress regulation in *Caenorhabditis elegans*. Mech Ageing Dev. 2003;124: 43–48.

89. Honda Y, Honda S. The daf-2 gene network for longevity regulates oxidative stress resistance and Mn-superoxide dismutase gene expression in *Caenorhabditis elegans*. FASEB J. 1999;13: 1385–1393.

90. Schieber M, Chandel NS. ROS function in redox signaling and oxidative stress. Curr Biol. 2014;24: R453-62.

91. Mustafi SB, Chakraborty PK, Dey RS, Raha S. Heat stress upregulates chaperone heat shock protein 70 and antioxidant manganese superoxide dismutase through reactive oxygen species (ROS), p38MAPK, and Akt. Cell Stress Chaperones. 2009;14: 579.

92. Hideg E, Jansen MAK, Strid A. UV-B exposure, ROS, and stress: inseparable companions or loosely linked associates? Trends Plant Sci. 2013;18: 107–115.

93. Zhou KI, Pincus Z, Slack FJ. Longevity and stress in *Caenorhabditis elegans*. Aging . 2011;3: 733–753.

94. Ristow M. Unraveling the truth about antioxidants: mitohormesis explains ROS-induced health benefits. Nat Med. 2014;20: 709–711.

95. Hahm J-H, Jeong C, Lee W, Koo HJ, Kim S, Hwang D, et al. A cellular surveillance and defense system that delays aging phenotypes in *C. elegans*. Aging . 2020;12: 8202–8220.

96. Wang H, Webster P, Chen L, Fisher AL. Cell-autonomous and non-autonomous roles of daf-16 in muscle function and mitochondrial capacity in aging *C. elegans*. Aging . 2019;11: 2295–2311.

97. Breckenridge DG, Kang B-H, Kokel D, Mitani S, Staehelin LA, Xue D. *Caenorhabditis elegans* drp-1 and fis-2 regulate distinct cell-death execution pathways downstream of ced-3 and independent of ced-9. Mol Cell. 2008;31: 586–597.

98. Gaffney CJ, Pollard A, Barratt TF, Constantin-Teodosiu D, Greenhaff PL, Szewczyk NJ. Greater loss of mitochondrial function with ageing is associated with earlier onset of sarcopenia in *C. elegans*. Aging . 2018;10: 3382.

99. Tang X, Luo Y-X, Chen H-Z, Liu D-P. Mitochondria, endothelial cell function, and vascular diseases. Front Physiol. 2014;5: 175.

100. Detaille D, Pasdois P, Sémont A, Dos Santos P, Diolez P. An old medicine as a new drug to prevent mitochondrial complex I from producing oxygen radicals. PLoS One. 2019;14: e0216385.

101. Lay S, Sanislav O, Annesley SJ, Fisher PR. Mitochondrial Stress Tests Using Seahorse Respirometry on Intact Dictyostelium discoideum Cells. Methods Mol Biol. 2016;1407: 41–61.

102. Zimmermann J, Obeng N, Yang W, Pees B, Petersen C, Waschina S, et al. The functional repertoire contained within the native microbiota of the model nematode *Caenorhabditis elegans*. ISME J. 2020;14: 26–38.

103. Michelsen KS, Aicher A, Mohaupt M, Hartung T, Dimmeler S, Kirschning CJ, et al. The role of toll-like receptors (TLRs) in bacteria-induced maturation of murine dendritic cells (DCS) Peptidoglycan and lipoteichoic acid are inducers of DC maturation and require TLR2. J Biol Chem. 2001;276: 25680–25686.

104. Schwandner R, Dziarski R, Wesche H, Rothe M, Kirschning CJ. Peptidoglycan- and lipoteichoic acid-induced cell activation is mediated by toll-like receptor 2. J Biol Chem. 1999;274: 17406–17409.

105. Brash DE, Haseltine WA. UV-induced mutation hotspots occur at DNA damage hotspots. Nature. 1982;298: 189–192.

106. Rittié L, Fisher GJ. UV-light-induced signal cascades and skin aging. Ageing Res Rev. 2002;1: 705–720.

107. Ikehata H, Ono T. The mechanisms of UV mutagenesis. J Radiat Res. 2011;52: 115–125.

108. Wlaschek M, Tantcheva-Poór I, Naderi L, Ma W, Schneider LA, Razi-Wolf Z, et al. Solar UV irradiation and dermal photoaging. J Photochem Photobiol B. 2001;63: 41–51.

109. Prasanth MI, Gayathri S, Bhaskar JP, Krishnan V, Balamurugan K. Understanding the role of p38 and JNK mediated MAPK pathway in response to UV-A induced photoaging in *Caenorhabditis elegans*. J Photochem Photobiol B. 2020;205: 111844.

110. Momma K, Homma T, Isaka R, Sudevan S, Higashitani A. Heat-Induced Calcium Leakage Causes Mitochondrial Damage in *Caenorhabditis elegans* Body-Wall Muscles. Genetics. 2017;206: 1985–1994.

111. Belhadj Slimen I, Najar T, Ghram A, Dabbebi H, Ben Mrad M, Abdrabbah M. Reactive oxygen species, heat stress and oxidative-induced mitochondrial damage. A review. Int J Hyperthermia. 2014;30: 513–523.

112. Henderson ST, Johnson TE. daf-16 integrates developmental and environmental inputs to mediate aging in the nematode *Caenorhabditis elegans*. Curr Biol. 2001;11: 1975–1980.

113. Rhee SG. Redox signaling: hydrogen peroxide as intracellular messenger. Exp Mol Med. 1999;31: 53–59.

114. Ali S, Jain SK, Abdulla M, Athar M. Paraquat induced DNA damage by reactive oxygen species. Biochem Mol Biol Int. 1996;39: 63–67.

115. Doonan R, McElwee JJ, Matthijssens F, Walker GA, Houthoofd K, Back P, et al. Against the oxidative damage theory of aging: superoxide dismutases protect against oxidative stress but have little or no effect on life span in *Caenorhabditis elegans*. Genes Dev. 2008;22: 3236–3241.

116. Sakamoto T, Maebayashi K, Nakagawa Y, Imai H. Deletion of the four phospholipid hydroperoxide glutathione peroxidase genes accelerates aging in *Caenorhabditis elegans*. Genes Cells. 2014;19: 778–792.

117. Detienne G, Van de Walle P, De Haes W, Schoofs L, Temmerman L. SKN-1-independent transcriptional activation of glutathione S-transferase 4 (GST-4) by EGF signaling. Worm. 2016;5: e1230585.

118. Curtis R, O'Connor G, DiStefano PS. Aging networks in *Caenorhabditis elegans*: AMP-activated protein kinase (aak-2) links multiple aging and metabolism pathways. Aging Cell. 2006;5: 119–126.

119. Vellai T, Takacs-Vellai K, Zhang Y, Kovacs AL, Orosz L, Müller F. Genetics: influence of TOR kinase on lifespan in *C. elegans*. Nature. 2003;426: 620.

120. MacNeil LT, Watson E, Arda HE, Zhu LJ, Walhout AJM. Diet-induced developmental acceleration independent of TOR and insulin in *C. elegans*. Cell. 2013;153: 240–252.

121. Zhou G, Huang C, Xing L, Li L, Jiang Y, Wei Y. Methionine increases yolk production to offset the negative effect of caloric restriction on reproduction without affecting longevity in *C. elegans*. Aging . 2020;12: 2680−2697.

122. Meissner B, Boll M, Daniel H, Baumeister R. Deletion of the intestinal peptide transporter affects insulin and TOR signaling in *Caenorhabditis elegans*. J Biol Chem. 2004;279: 36739–36745.

123. Doherty TJ. Invited review: Aging and sarcopenia. J Appl Physiol. 2003;95: 1717–1727.

124. Morley JE, Argiles JM, Evans WJ, Bhasin S, Cella D, Deutz NEP, et al. Nutritional Recommendations for the Management of Sarcopenia. J Am Med Dir Assoc. 2010;11: 391–396.

125. Taaffe DR. Sarcopenia--exercise as a treatment strategy. Aust Fam Physician. 2006;35: 130–134.

126. Ashrafi K. Obesity and the regulation of fat metabolism. WormBook. 2007; 1–20.

127. Srinivasan S. Regulation of Body Fat in *Caenorhabditis elegans*. Annu Rev Physiol. 2015;77: 161–178.

128. Liu Y, Fiskum G, Schubert D. Generation of reactive oxygen species by the mitochondrial electron transport chain. J Neurochem. 2002;80: 780–787.

129. St-Pierre J, Buckingham JA, Roebuck SJ, Brand MD. Topology of superoxide production from different sites in the mitochondrial electron transport chain. J Biol Chem. 2002;277: 44784–44790.

130. Schon EA, Santra S, Pallotti F, Girvin ME. Pathogenesis of primary defects in mitochondrial ATP synthesis. Semin Cell Dev Biol. 2001;12: 441–448.

131. Luz AL, Lagido C, Hirschey MD, Meyer JN. In Vivo Determination of Mitochondrial Function Using Luciferase-Expressing *Caenorhabditis elegans*: Contribution of Oxidative Phosphorylation, Glycolysis, and Fatty Acid Oxidation to Toxicant-Induced Dysfunction. Curr Protoc Toxicol. 2016;69: 25.8.1-25.8.22.

132. Dudkina NV, Kouril R, Peters K, Braun H-P, Boekema EJ. Structure and function of mitochondrial supercomplexes. Biochim Biophys Acta. 2010;1797: 664–670.

133. Cogliati S, Frezza C, Soriano ME, Varanita T, Quintana-Cabrera R, Corrado M, et al. Mitochondrial cristae shape determines respiratory chain supercomplexes assembly and respiratory efficiency. Cell. 2013;155: 160–171.

134. Acín-Pérez R, Fernández-Silva P, Peleato ML, Pérez-Martos A, Enriquez JA. Respiratory active mitochondrial supercomplexes. Mol Cell. 2008;32: 529–539.

135. Tanner CM, Kamel F, Ross GW, Hoppin JA, Goldman SM, Korell M, et al. Rotenone, paraquat, and Parkinson's disease. Environ Health Perspect. 2011;119: 866–872.

136. Sherer TB, Betarbet R, Testa CM, Seo BB, Richardson JR, Kim JH, et al. Mechanism of toxicity in rotenone models of Parkinson's disease. J Neurosci. 2003;23: 10756–10764.

137. Cannon JR, Tapias V, Na HM, Honick AS, Drolet RE, Greenamyre JT. A highly reproducible rotenone model of Parkinson's disease. Neurobiol Dis. 2009;34: 279–290.

138. Morris ME. Movement disorders in people with Parkinson disease: a model for physical therapy. Phys Ther. 2000;80: 578–597.

139. Kösel S, Hofhaus G, Maassen A, Vieregge P, Graeber MB. Role of mitochondria in Parkinson disease. Biol Chem. 1999;380: 865–870.

140. Thomas B, Beal MF. Parkinson's disease. Hum Mol Genet. 2007;16 Spec No. 2: R183-94.

141. Sherer TB, Betarbet R, Greenamyre JT. Environment, mitochondria, and Parkinson's disease. Neuroscientist. 2002;8: 192–197.

142. Perez-Pardo P, Dodiya HB, Engen PA, Naqib A, Forsyth CB, Green SJ, et al. Gut bacterial composition in a mouse model of Parkinson's disease. Benef Microbes. 2018;9: 799–814.

143. Imai Y, Inoshita T, Meng H, Shiba-Fukushima K, Hara KY, Sawamura N, et al. Light-driven activation of mitochondrial proton-motive force improves motor behaviors in a Drosophila model of Parkinson's disease. Commun Biol. 2019;2: 424.

144. Singleton AB, Farrer M, Johnson J, Singleton A, Hague S, Kachergus J, et al. [alpha]-synuclein locus triplication causes Parkinson's disease. Science. 2003;302: 841.

145. Stefanis L. α-Synuclein in Parkinson's disease. Cold Spring Harb Perspect Med. 2012;2: a009399.

146. Kuwahara T, Koyama A, Gengyo-Ando K, Masuda M, Kowa H, Tsunoda M, et al. Familial Parkinson Mutant α-Synuclein Causes Dopamine Neuron Dysfunction in Transgenic *Caenorhabditis elegans*. J Biol Chem. 2006;281: 334–340.

147. Marcinko K, Steinberg GR. The role of AMPK in controlling metabolism and mitochondrial biogenesis during exercise. Exp Physiol. 2014;99: 1581–1585.